IONOSPHERIC COMMUNICATIONS ENHANCED PROFILE ANALYSIS & CIRCUIT

(ICEPAC)

PREDICTION PROGRAM

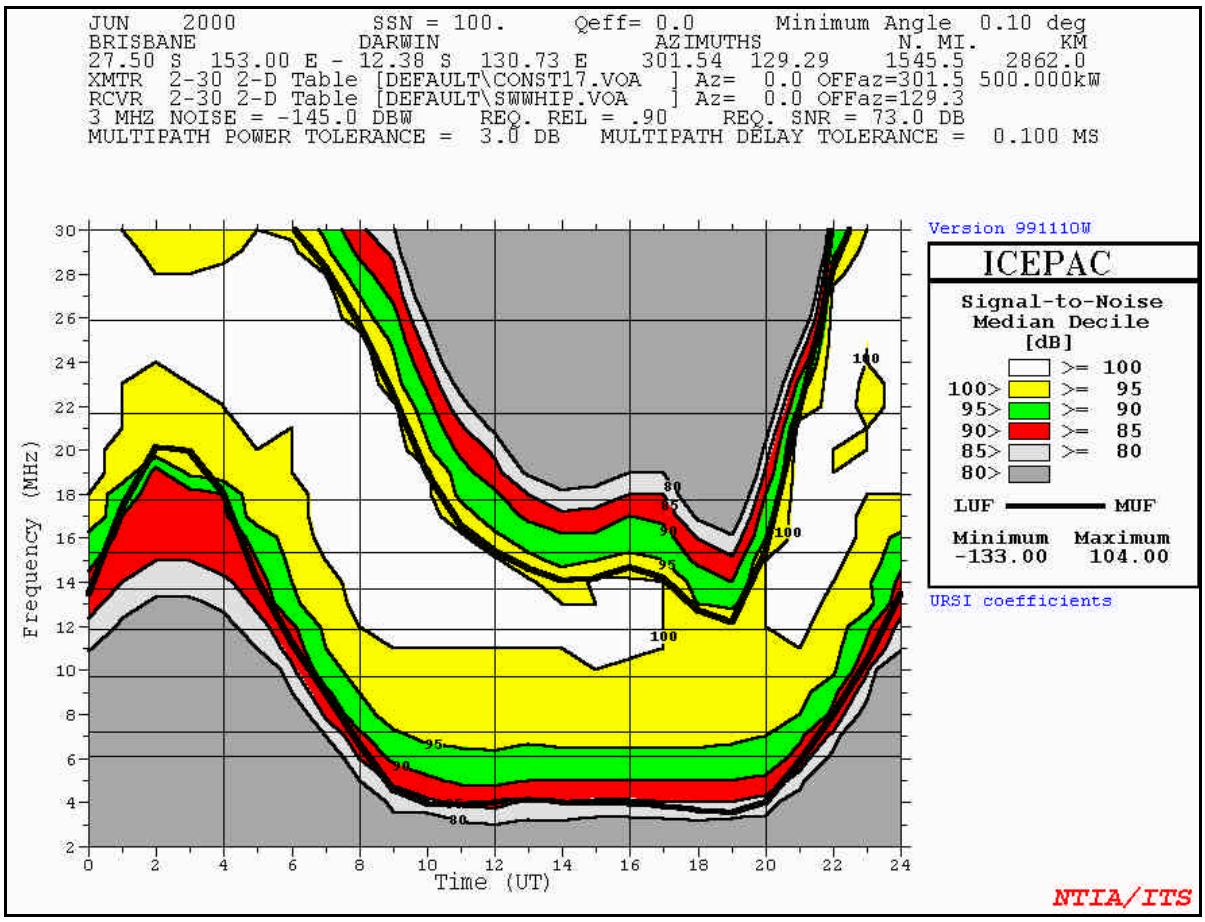

TECHNICAL MANUAL

TABLE OF CONTENTS

TABLE OF CONTENTS (CONT'D)

TECHNICAL DESCRIPTION OF ICEPAC PROPAGATION PREDICTION PROGRAM

FRANK G. STEWART

Simulation models have been developed for predicting and analyzing the performance of HF systems that depend on ionospheric propagation. These models are documented.

1. INTRODUCTION

This report describes a propagation predictions model (ICEPAC) that is an extension of the IONCAP program. It differs in the polar region structure of the ionosphere and the low and mid latitude ionospheric structure. The ICED (ionospheric conductivity and electron density) profile model is a statistical model of the large-scale features of the northern hemisphere ionosphere. The model recognizes the different physical processes that exist in the different regions of the ionosphere. It contains distinct algorithms for the subauroral trough, the equator-ward portion of the auroral zone, the polward region of the auroral zone, and the polar cap. This report will be a complete description of the ICEPAC propagation prediction program.

The predictions are used primarily for long-term (month-to-month, year-to-year, etc.) frequency management and circuit planning, but are often used for hour-to-hour and day-to-day operations as well. Most important, propagation considerations are basic to studies of electromagnetic compatibility, and analytical computer prediction methods such as the one described in this report are essential to a practical solution.

It should be emphasized that a computer program is a tool for convenience in calculation; the user must exercise his own engineering judgment in determining the applicability and limitation of the results to specific problems.

1.1 HF RADIO PROPAGATION HISTORY

For many years, numerous organizations have been employing the High Frequency (HF) spectrum to communicate over long distances. It was recognized in the late 30's that these communication systems were subject to marked variations in performance, and it was hypothesized that most of these variations were directly related to changes in the ionosphere. Considerable effort was made in the United States, as well as in other countries, to investigate ionospheric parameters and determine their effect on radio waves

and the associated reliability of HF circuits. A worldwide network of vertical incidence sounders was established to measure values of parameters such as foE, foF1, foEs, foF2, and h'F. Worldwide noise measurement records were started and steps were taken to record observed variations in signal amplitudes over various HF paths. The results of this research established that ionized regions ranging from approximately 70 to 1000 km above the earth's surface provide the medium of transmission for electromagnetic energy in the HF spectrum (2 to 30 MHz) and that most variations in HF system performance are directly related to changes in these ionized regions. The ionization is produced in a complex manner by the photoionization of the earth's high altitude atmosphere by solar radiation. Within the ionosphere, the recombination of the ions and electrons proceeds slowly enough (due to low gas densities) so that some free electrons persist even throughout the night. In practice, the ionosphere has a lower limit of 50 to 70 km and no distinct upper limit, although 1000 km is somewhat arbitrarily set as the upper limit for most application purposes.

The vertical structure of the ionosphere is changing continuously. It varies from day to night, with the seasons of the year, and with latitude. Furthermore, it is sensitive to enhanced periods of short-wavelength solar radiation accompanying solar activity. In spite of all this, the essential features of the ionosphere are usually identifiable, except during periods of unusually intense geomagnetic disturbances.

The Radio Propagation Unit of the U.S. Army Signal Corps provided a great deal of information and guidance on the phenomena of HF propagation in 1945. By 1948, a treatise of ionospheric radio propagation was published by the Central Radio Propagation Laboratory (CRPL) of the national Bureau of Standards. This document (NBS, Circular 462, 1948) outlined the state of the art in HF propagation. Techniques were included for: predicting the maximum usable frequencies (MUF); determining the MUF for any path at any time taking into account the various possible modes of propagation by combining theory and operational experiences; and estimating skywave field strength.

Laitinen and Haydon (1962) of the U.S. Army signal Radio Propagation Agency furthered the science of predicting HF system performance by developing empirical ionospheric absorption equations and combining them with the theoretical ground loss, free-space loss, and antenna gain factors so that expected field strengths could be estimated for radio signals reflected from the E- and F2-regions, considering the effect of solar activity and seasonal and diurnal variations.

In the United States, the first automated HF path prediction computer program was developed in 1957, for the U.S. Army Signal Corps, Radio Propagation Agency (Contract DA 360039 SC-66438), now part of the U.S. Army Strategic Communications Command (see Stanford Research Institute (SRI), 1957). A later version was published in 1961 (Radio Corporation of America, 1961). The first fully automated program, in which the oblique transmission equations for parabolic layers were used, was developed in 1966 (Lucas and Haydon, 1966) by ESSA's Institute for Telecommunication Sciences and Aeronomy (ITSA), which preceded the Institute for Telecommunication Sciences (ITS).

This work was continued in two separate paths, one for communications analysis and predictions, reported in ITS-78 (Barghausen et al., 1969) and another for analysis and prediction of OTH radar systems reported in NRL Tech. Reports 2226 and 2500 (Headrick et al., 1971; Lucas et al., 1972).

The culmination of this work was the IONCAP program which uses the above described development for the shorter paths and other techniques for the long path predictions (Whale, 1969).

Fundamental to all efficient HF computer prediction programs are the synoptic numerical coefficient representations of the ionospheric characteristics. These were first developed by ITSA (formerly the Central Radio Propagation laboratory, National Bureau of Standards) and first published in 1960 (Jones and Gallet, 1960). Subsequent modification led to the technique now used (Jones et al., 1966), which will be discussed later.

1.2 GENERAL DESCRIPTION

The techniques used in the computer program described in this report are procedurally similar to the earlier ITS programs (ITSA-1, ITS-78, HFMUFES, IONCAP), but there have been sufficient significant changes to warrant further documentation.

The literature on the ionosphere and its role in HF sky-wave radio communications is very extensive. Theories concerning ionospheric propagation will not be repeated here in detail, but some background material will be given where necessary for an understanding of the prediction processes and the philosophy of the program.

In the basic model, it is assumed that the ionosphere can be represented by one or more Chapman layers (Dudney, 1983), given sufficient information concerning the height of maximum ionization, semi-thickness, and electron density. Sufficient data must be available to predict an average electron density distribution with height for any possible transmission path. The

model retains the equivalent path theorem (Breit and Tuve, 1926; Martyn, 1935) and its transmission curve solution (Smith, 1939), since this is the method for scaling and predicting ionospheric characteristics.

The program predicts the long-term operational parameters, such as maximum usable frequency (MUF), optimum traffic frequency (FOT), and lowest useful frequency (LUF), in terms of the probability of successful transmission for a particular circuit. The probability of successful transmission depends on the probability that the transmission frequency is below the critical frequency (i.e., the maximum frequency for reflection) of the F2 layer and the probability that the available signal-to-noise ratio is above a specified level.

Throughout the report, attempts have been made to clarify duplication of nomenclature and symbols commonly accepted in wave propagation and antenna studies.

2. PREDICTABLE IONOSPHERIC PARAMETERS

The presence of free electrons in the ionosphere produces the reflecting regions important to High Frequency (HF) radio-wave propagation. In the principal regions, between the approximate heights of 75 km and 500 km, the electrons are produced by the ionizing effect of ultraviolet light and soft x-rays from the sun. for convenience in studies of radio-wave propagation, the ionosphere is divided into three regions defined according to height and ion distribution: the D,E, and F regions. Each region is subdivided into layers called the D,E, Es, F1, and F2 layers, also according to height and ion distribution. These are not distinctly separated layers, but rather overlapping regions of ionization that vary in thickness from a few kilometers to hundreds of kilometers. The number of layers, their heights, and their ionization (electron) density vary both geographically and with time. At HF, all the regions are important and must be considered in predicting the operational parameters of radio communication circuits.

2.1 The D Region

The D region lies between the approximate limits of 75 and 90 km above the earth's surface. The electron density is relatively small compared with that of the other regions, but, because of collisions between the molecules of the atmosphere and free electrons excited by the presence of an electromagnetic wave, pronounced energy loss occurs. This energy loss, dissipated in the form of thermal energy of the electrons or thermal (electromagnetic) noise, is termed absorption. Absorption in the D region is called non-deviative, since it occurs below the level of reflection and predominates when the real part of the refractive index is near unity ($\mu \approx 1$); i.e., little or no bending takes place. Higher in the E and F regions, electron collisions with atmosphere molecules can also affect the condition for reflection that occurs wherever there is a marked bending of the wave. This is explained by the fact that as the wave nears its reflecting level, there is a slowing down or retardation effect, which allows additional time for collisions to occur and thus for absorption to take place. Absorption of this type is called deviative absorption.

Because of the low electron density, the D region does not reflect useful transmissions in the frequency range above 1 MHz. However, D-region absorption is important at all frequencies and, because its ionization is produced by ultraviolet solar radiation, it is primarily a daytime phenomenon. The degree

of absorption, expressed by the absorption factor, is proportional to the product of the collision frequency and electron density, and approximately inversely proportional to the square of the wave frequency. The absorption factor variation is adequately represented by cos χ, where χ is the zenith angle of the sun. After sunset in the D region, ionization decreases rapidly and non-deviative absorption becomes negligible 2 to 3 hours later.

Non-deviative D-region absorption is the principal cause of the attenuation of HF sky waves, particularly at the lower frequencies during daylight hours. It is accounted for in the program by an analytical, semi-empirical expressions, which is explained in detail in section 5. Deviative absorption losses are estimated and included in the loss calculations as an uncertainty factor (see sec.7).

Another important property of the upper D and lower E regions is the differential absorption between the ordinary and extraordinary waves produced by the earth's magnetic field. These differential absorption properties of the characteristic waves and their down-coming state of polarization are especially important at frequencies below about 3 MHz and in low-latitude regions. In these areas, when vertically polarized antennas are used, most of the radiated power is coupled into the extraordinary wave (Berghausen, 1966). The extraordinary wave is reflected at a lower level, its critical frequency is somewhat higher, and it suffers greater absorption. The idealized situation is when a vertically polarized wave is transmitted in an easterly or westerly direction along the location of the earth's magnetic dip equator and the wave frequency is exactly equal to the gyromagnetic frequency (~0.8 MHz). Then, all the radiated power is coupled into the extraordinary wave and the ordinary wave does not exist. In this program, only the ordinary wave critical frequency and absorption properties are considered.

2.2 THE E REGION

For communication, the most important characteristic feature of the E region is the temporal and geographic variation of its critical frequency. In almost all other respects, the features of the E layer are very predictable compared with those of the F2 layer.

2.2.1 Measurements

A large volume of vertical-incidence ionosonde data has been collected over about three solar cycles, and many features of the E region are therefore well known. The minimum virtual height of the E region and the variation of

maximum electron density within this region as a function of time and geographic location are readily obtained from the ionograms. The phenomenology of sporadic-E has been investigated, but classification of sporadic-E types remain unresolved. The effects of different types of sporadic-E on oblique-incidence radio propagation are not established; as a result, the compilation of meaningful statistics to form the basis of predictions is difficult.

The E-region characteristics that have been systematically scaled from the vertical-incidence ionosonde records include:

foE — The critical frequency of the ordinary component of the E layer; i.e., that frequency at which the signal from the ionosonde just penetrates the E layer.

h'E — The minimum virtual height of the E layer, measured at the point where the trace becomes horizontal.

foEs — The highest observed frequency of the ordinary component of sporadic-E (Es).

h'Es — The minimum virtual height of the sporadic-E layer, measured at the point where the trace becomes horizontal.

fbEs — The blanketing frequency; i.e., the lowest ordinary wave frequency at which the Es layer begins to become transparent, usually determined from the minimum frequency at which ordinary wave reflections of the first order are observed from a higher layer.

2.2.2 Predictions

The regular E layer is predicted using three parameters: the monthly median value of critical frequency (foE), height of maximum ionization of the layer (hmE), and ratio of hmE to semi-thickness (ymE). In the past, the E-layer critical frequency has been determined by a semi-empirical equation involving the sunspot number and the zenith angle of the sun. Obviously, such a relationship would be inadequate to estimate foE values at sunrise or sunset and during nighttime. Worldwide numerical coefficients of monthly median foE are available for computer applications in terms of geographic latitude, longitude, and universal time. The numerical coefficients (Leftin, 1976)

representing foE were derived from measurements taken during 1958 and 1964. These years were selected for analysis because the data are representative of the high (1958) and low (1964) phases of the sunspot cycle. Linear interpolation is used between the representative data for the high (SSN = 150) and low (SSN = 10) sunspot periods to obtain foE estimates at all other phases of the solar cycle.

Little information is available concerning the statistical distribution of the monthly median foE. In daytime, the E layer is sufficiently regular that the distribution spread of the monthly median foE may be considered negligible. Nighttime data are insufficient, but it appears justified (Elling, 1961; Wakai, 1966; Wakai, 1967) to assume a similar regularity for the foE monthly median of the nighttime E layer.

Therefore, we believe that the E-layer characteristics most important for communication purposes are adequately represented by the available foE monthly median numerical coefficients. The approximate true height range of the regular E layer is well established at 90 to 130 km and it is assumed that the maximum electron density occurs at 110 km and the semi-thickness is 20 km (Kneckt, 1963; Frihagen, 1965). With the above assumption, the ratio of the height to the semi-thickness (hmE/ymE) is assumed to be 5.5.

2.3 THE F REGION

The vertical-incidence ionosonde network with its long series of measurements over much of the world, provides the basis for F-region predictions (Martyn, 1959). The following parameters have been systematically scaled from the vertical ionosonde records (Piggott and Rawer, 1961), although some stations do not report all of them:

foF2 — The critical frequency of the ordinary component of the F2 layer; i.e., that frequency at which the signal from the ionosonde just penetrates the F2 layer.

M(3000)F2 — The factor for converting vertical-incidence critical frequencies to oblique incidence for a distance of 3000 km via the F2 layer.

foF1 The critical frequency of the ordinary component of the F1 layer; i.e., that frequency at which the signal from the ionosonde just penetrates the F1 layer.

H'F2 The minimum virtual height of the F layer; i.e., the minimum virtual height of the night F layer and the day F1 layer. It is measured at the point where the F trace becomes horizontal. (In earlier years the minimum virtual height of the night F layer was often combined with that of the day F2 layer, the combined tabulation being designated h'F2. In these cases, the minimum virtual height of the F1 layer, h'F1, was tabulated separately.)

hpF2 The virtual height of the F2 layer corresponding to a frequency f, where f = 0.834 foF2. This is based on the assumption of a parabolic ionization distribution, which is usually considered justified as an approximation to the height of maximum ionization of the F2 layer.

For HF radio communications, the F region is the most important part of the ionosphere. It is not regular and because of its variability, short time scale estimates of the important F-region characteristics are required if predictions of the operational parameters of HF radio systems are to be meaningful.

There are many characteristic features of the F region important to HF radio communications. It is beyond the scope of this report to describe all of them, nor is this necessary, since there are many publications and excellent textbooks on the subject. We will briefly describe only those F-region characteristics that are relevant to the program.

The F1 layer has not been as well defined as the F2 layer in terms of its predictable characteristic features. the F1 layer is of importance to communication only during daylight hours or during ionospheric storms (Kelso, 1964; Wright et al., 1960-63); it lies in the height range of about 200 to 250 km and undergoes both seasonal and solar cycle variations, which are more pronounced during the summer and in high sunspot periods.

2.3.2 Predictions

The F2 layer is described by three parameters: monthly median value of critical frequency (fof2), height of maximum ionization (hmF2), and a ratio of hmF2 to semi-thickness (ymF2). Monthly median values of foF2 and the M(3000)F2 for two solar activity levels are available as numerical coefficients in terms of a modified magnetic-dip angle and longitude, and universal time (CCIR, 1966). There is also available a more recent model of the F2 region of the ionosphere. This model is based on a combination of observed and theoretical data. The theoretical data provided stability in large regions where no observed data existed, such as ocean areas and non-industrialized areas. (CCIR 1989) This F2 region model showed minor improvements in populated regions and significant improvements over sea area and unpopulated regions when compared to observed ionosound and satellite measurements. For this document the old CCIR model will be described. The analytical structure of the more recent coefficients and the documentation would be consistent. The solar activity dependence is accounted for by linear interpolation.

The model divides the F2 region into four distinct zones: (1) normal low-latitude and mid-latitude ionosphere as described by the numerical coefficients, (2) the trough, (3) the zone of aurorally enhanced foF2's and (4) the polar cap. The key boundary for the model is the equatorward edge of the auroral oval. The resulting boundary location is parameterized by comparing it with standard Feldstein oval boundaries computed as a function of Kp or Q (Whalen, 1972). The resulting magnetic index (Kp_{eff} or Q_E) is an effective auroral energy index because it is based on the "current" state of the high latitude ionosphere.

2.4 PROPAGATION BY WAY OF SPORADIC E AND OTHER ANOMALOUS IONIZATION

In the preceding discussion of the important regions of the ionosphere, we concentrated on the first order characteristics of the various layers. There are many other characteristic phenomena, e.g., sporadic E, spread F, F scatter, multiple traces, and other transients, often observed on ionosonde records (Piggott and Rawer, 1961), that are important in radio communications; however, present prediction schemes demand that the general ionospheric structure be statistically representative and in a continuous sequence. Of these phenomena, the only one we have been able to partly represent for prediction purposes is the sporadic-E layer.

2.4.1. Sporadic E

Sporadic E (Smith and Matsushita, 1962; Bowhill, 1966; Whitehead, 1969) is seen on vertical and oblique ionograms near the height of maximum ionization of the regular E layer. Sporadic E(Es) is characterized by little or no retardation at its critical frequency and may be either blanketing (totally reflecting) or semitransparent (partly reflecting), or both, up to very high frequencies(>75 MHz). These characteristics can be helpful or harmful to radio communications. For example, blanketing Es may block propagation via a more favorable regular layer mode in a certain frequency range or cause additional attenuation at other frequencies. Partially reflecting Es can cause serious multipath and mode interference, especially detrimental to data transmission systems. However, Es may extend the useful frequency range and its presence can be effectively used in system design and operations.

The physical processes that produce sporadic-E ionization are not fully known, but it is generally accepted that the mechanisms may be quite different in auroral, temperate, and equatorial geographic areas (Bowhill, 1966; Whitehead, 1969). In auroral areas, energetic particles appear to play a vital role in the production of sporadic E (Baily, 1968). Temperate-area Es is best explained by the behavior of upper atmosphere winds (Matsushita and Reddy, 1968) and a related wind-shear theory (Axford and Cunnold, 1968). In equatorial areas, i.e., in a narrow $\pm 6^{o}$ belt centered on the magnetic dip equator, the production of sporadic-E is explained by theories on plasma instability phenomena (Farley, 1963; Waldteufel, 1965). Methods of forecasting sporadic E are influenced by the physical processes involved and should be considered in all prediction schemes. In this report, we are not directly concerned with forecasting techniques, but with predicting operational parameters when sporadic E is the dominant propagation mode. Therefore, the numerical coefficients representing the monthly statistical distribution of foEs for any location are empirically derived estimates of sporadic E during periods of solar cycle minimum and maximum, and they are used only when propagation via the regular E layer is not possible (see sec. 3).

It may be helpful to review the general occurrence characteristics of sporadic E for the three geographic areas mentioned above (CCIR, 1969):

Auroral Es - Occurs mainly at night at geomagnetic latitudes greater than about 60^{o}, with a maximum near 69^{o}. Its seasonal, diurnal, and solar cycle patterns are not clear. It occurs more frequently during periods of high magnetic activity and follows the sudden commencement associated with a solar flare (Hunsucker and Bates, (1969).

Temperate Es - Characterized by a pronounced maximum during the summer solstices (June-July in the Northern Hemisphere and December-January in the Southern Hemisphere). A seasonal minimum occurs during the vernal equinox; this minimum changes abruptly at 60^o geomagnetic latitude. The diurnal pattern exhibits peaks during mid-morning hours and near sunset. It is primarily observed during the daylight hours and shows a complicated dependence on the sunspot cycle.

Equatorial Es - A regular daytime occurrence without seasonal dependence. It is highly transparent (partly reflecting) and reaches high ($\approx$ 50 MHz) frequencies. Values of foEs around 10 MHz are regularly observed by ionosondes near the geomagnetic dip equator. The reflection properties depend on the direction of propagation; higher reflection coefficients are to be expected for north-south paths.

2.4.2 PREDICTIONS

Numerical coefficients are available for each month representing the median and decile values of foEs in terms of a modified magnetic-dip angle and longitude, and universal time (Leftin et al., 1968). These numerical maps are from data taken during periods of solar activity minimum (1954) and solar activity maximum (1958). Linear interpolation is used for other levels of solar activity. Unless other information is available, the virtual height of the sporadic-E layer is assumed to be 110 km.

2.5 ELECTRON DENSITY PROFILE MODEL

Frequency versus virtual height traces of the ordinary wave as available on vertical incidence ionograms can be converted into electron density profiles by a standard reduction program. These profiles, including geographic, diurnal, seasonal, and solar cycle variations, are generated between heights of 70 km and the height of maximum of the F2 layer, hmF2. The electron density is given by the relationship

$$N = 1.24 \times 10^{10} f_N^2 \quad (4)$$

N = electrons per cubic meter

f_N = plasma frequency MHz

A fixed reflection height for the E and F2 layers was used in the original computer program (Lucas and Haydon, 1961). Then parabolic layers for both the E and F2 layer were used (Lucas and Haydon, 1966; Barghausen et al., 1969). The F1 layer was added and the profile was generated by taking the maximums of these intersecting layers. The current method of profile

generations replaces the parabolic layer structure with a Chapman layer structure. The parabolic layer is analytically more tractable but the Chapman layer has the advantage that a layer whose process is dominated by electromagnetic ionization and chemical losses is closely described by the Chapman layer. In addition, the Chapman layer decreases exponentially with altitude above the layer peak -- this again more closely describes the ionospheric situation. (Dudney 1983).

3. CALCULATION OF CIRCUIT PARAMETERS FROM PATH GEOMETRY

To determine the operational parameters for an HF ionospheric radio communication circuit, it is necessary to calculate several parameters that are based on the geometry of the path, such as path length, path bearings, and zenith angle of the sun.

3.1 PATH LENGTH AND BEARINGS

The first parameter to be calculated, given the geographic latitude and longitude of the transmitting and receiving locations, is the path length, which is taken to be the shorter of the great-circle distances between the two points, and which is computed as follows:

$$\cos d = \sin x_1 \sin x_2 + \cos x_1 \cos x_2 \cos(y_1 - y_2), \quad (3.1)$$

where

x_1 = geographic latitude of transmitter,
y_1 = geographic longitude of transmitter,
x_2 = geographic latitude of receiver,
y_2 = geographic longitude of receiver,
d = path length in radians.

Having obtained the path length, we calculate the bearing of transmitter to receiver and receiver to transmitter along the great circle path:

$$\cos b_1 = (\sin x_2 - \sin x_1 \cos d)/ (\cos x_1 \sin d) \quad (3.2)$$

$$\cos b_2 = (\sin x_1 - \sin x_2 \cos d)/ (\cos x_2 \sin d) \quad (3.3)$$

where

b_1 = bearing transmitter to receiver in radians,
b_2 = bearing receiver to transmitter in radians.

3.2 REFLECTION AREA COORDINATES

In the development of a profile of electron density along the path, the ionospheric parameters at from one to five reflection areas along the path are evaluated depending on the path length. These five areas are:

1. The midpoint of the path.
2. The E-region reflection area nearest the transmitter for the estimated least possible number of hops.

3. The E-region reflection area nearest the receiver for the same number of hops.
4. The F-region reflection area nearest the transmitter for the estimated least possible number of hops.
5. the F-region reflection area nearest the receiver for the same number of hops.

The estimated least possible number of E-layer and F-layer hops is determined from the following relationship to path length:

1E, 1F - 0000 km $\leq$ path length < 2000 km.
2E, 1F - 2000 km $\leq$ path length < 4000 km.
4E, 2F - 4000 km $\leq$ path length < 8000 km.
6E, 3F - 8000 km $\leq$ path length < 12,000 km.

for paths less than 2000 km, only the path midpoint is considered. This establishes the reflection areas for determining the ionospheric characteristics for the entire path.

To evaluate the ionospheric parameters of these five reflection areas, their geographic coordinates and geomagnetic latitude have to be computed as follows:

$$x_n = 90^o - \arccos(\cos d_n \sin x_1 + \sin d_n \cos x_1 \cos b_1) \quad (3.4)$$

$$y_n = y_1 - \arccos\left(\frac{\cos d_n - \sin x_n \sin x_1}{\cos x_n \cos x_1}\right) \quad (3.5)$$

$$g_n = 90^o - \arccos(\sin 78.5^o \sin x_n + \cos 78.5^o \cos x_n \cos (y_n - 69.0^o)), \quad (3.6)$$

where

d_n = angular distance of reflection area from transmitter,

x_n = geographic latitude of reflection area,

y_n = geographic longitude of reflection area,

g_n = geomagnetic latitude of reflection area.

The modified magnetic dip latitude is required at each control point for the evaluation of the ionospheric parameters. The magnetic dip is calculated from the 1963 Jensen and Cain model of the earth's magnetic field. (Jensen, D.C. and Cain, T.C.- 1962) The corrected geomagnetic latitude and longitude is required to define the location and structure of the polar ionosphere.

Computation of the corrected geomagnetic coordinates begins by starting in the equatorial plane at the same point with a dipole field line and a spherical analysis field line, and then calculating the distance between the "landing points" of the two field lines on the earth. In its simplest form, the method consists of labeling the spherical analysis field lines (sometimes called the real field lines) with the coordinates of the coincident equatorial, dipolar field lines. That is, the spherical analysis field has numerous irregularities due to regional anomalies and so it is difficult to assign a meaningful symmetric grid pattern to such a system. However, superimposing the symmetric dipolar grid system on the "realistic" spherical analysis produces a useful coordinate system for modeling purposes.

3.3 SUN'S ZENITH ANGLE

For the first three reflection areas, the zenith angle of the sun is needed for each hour of the day, to be used later in calculating the absorption factor, and is computed from the following equation:

$$\cos \chi = \sin x_n \sin s_x + \cos x_n \cos s_x \cos(s_y - y_n), \qquad (3.7)$$

where

t_g = universal time,

$s_y = 15\ t_g - 180$ = subsolar longitude,

s_x = subsolar latitude for the middle of the month,

χ = sun's zenith angle.

3.4 TYPES OF PATHS CONSIDERED

Up to six ray paths are evaluated for each hour and each designated frequency. These ray paths are interpolated from the reflectrix table for the frequency with the distance calculated using a corrected version of Martyn's Theorem for the equivalence of oblique and vertical heights of reflectivity.

3.5 IONOSPHERIC PARAMETERS

Once the propagation path has been located geographically, the parameters of the ionosphere at the reflection areas along the path are needed for further computation. These parameters are the critical frequency of the layer, height of the maximum electron density of the layer, height of the bottom of the layer, and semi-thickness of the layer.

3.5.1 Low and Mid Latitude Model

The critical frequency of the E layer (foE) is obtained from world maps (Leftin, 1976) and is the median value of that parameter. The height of the maximum foE (hmE) is set at 110 km for the low and mid latitude with the semi-thickness (ymE) set at

$$ymE = \frac{hmE}{5.5} = \frac{110}{5.5} = 20.0 \qquad (3.8)$$

The maximum solar zenith angle χ_{max} for the occurrence of the F1 layer is used as the cutoff for the prediction of the monthly median foF1. This is necessary since the F1 layer is normally observed on vertical incidence ionograms during daylight hours only. The χ_{max} and critical frequency of the F1 layer (foF1) are calculated as follows (Rosich et al., 1973)

$$\chi_{max} = AC_1 + BC_1 * SSN + (AC_2 + BC_2 * SSN) * \cos(GMDIP) \qquad (3.9)$$

where SSN = 12 month smoothed mean sunspot number

GMDIP = Rawer's modified magnetic dip latitude

AC_1, BC_2, AC_2, BC_2, are coefficients based on a two dimensional representation of χ_{max} using sunspot numbers and Rawer's modified magnetic dip. A set of coefficients exists for each month.

When χ at the control point is greater than χ_{max} then foF1 = 0.2

When χ at the control point is less than χ_{max} , the following equation is used:

$$foF1 = A_1 + B_1 * SSN + (A_2 + B_2 * SSN) \cos\chi + (A_3 + B_3 * SSN) \cos^2\chi \qquad (3.10)$$

where

SSN is the 12 month smooth mean sunspot number and

χ is the solar zenith angle of the sun at the control point ($\chi \leq 90.0$).

A_1, B_1, A_2, B_2, A_3, B_3 are coefficients from the numerical representations. (Rosich et. al. 1973). The height of the maximum ionization for the F_1 layer (hmF1) is calculated as follows:

hmF1 = 165 + 0.6428 * χ or 200 which ever is less

The semi-thickness of the foF1 layer (ymF1) is calculated as

$$ymF1 = hmF \frac{1}{4.0}$$

where χ is the solar zenith angle of the sun and hmF1 is restricted to a maximum value of 200 km.

The critical frequency of the F2 layer is obtained from world maps (Jones et al., 1966) and is the median value of that parameter. The true height of the maximum electron density of the F layer is developed in two steps. First, the M(3000)F2 factor is obtained from world maps, and then the true height of the maximum ionization hmF2 in the layer is calculated on the basis of the following relationship (Dudney, 1983):

XE = foF2/foE if XE < 1.7, XE = 1.7 (3.11)

$$\Delta m = \left(\frac{.253}{XE - 1.215} \right) - 0.012$$

(3.12)

$$F = M(3000)F2 \sqrt{\frac{0.0196 * M(3000)F\,2^2 + 1}{1.2967\, M(3000)F\,2^2 - 1}}$$

(3.13)

$$hmF2 = \frac{1490F}{M(3000)F2 + \Delta M} - 176$$

(3.14)

The semi-thickness (ymF2 of the F2 layer is calculated on the basis of coefficients that represent the ratio of the height of maximum ionization of the F2 region to its semi-thickness ymF2. (Lucas et al., 1966).

3.5.2 Auroral Zone

The Auroral foE is made up of both solar ionization and auroral zone precipitating particals. The maximum auroral critical frequency ($foEa_{max}$) due to precipitating particals (Vondrak et.al. 1978) is calculated by the following equation:

$$\begin{aligned} foEa_{max} &= 2.5 + Qe / 9.0 && 0 \le Qe \le 2.7 \\ &= -1.0 + 7/5\ Qe && 2.7 < Qe \le 4.2 \\ &= 3.2 + 2/5\ Qe && Qe > 4.2 \end{aligned} \qquad (3.15)$$

where Qe = effective geomagnetic activity index. $foEa_{max}$ is then adjusted for local time magnetic variations (Maximum ionizations at 0300 magnetic local time and minimum ionization at 1500 magnetic local time).

$$foEa_{\max} = foEa_{\max} - \frac{(TCGM - 3)}{12}(foEa - 1) \qquad TCGM \le 15$$

$$foEa_{\max} = foEa_{\max} - \frac{(27 - TCGM)}{12}(foEa - 1) \qquad TCGM > 15$$

(3.16)

where TCGM = time corrected geomagnetic time.

A linear interpolation is done between the oval boundaries and the point of maximum ionization in the oval. The FoEa values of the polarized and equatorial boundaries of the auroral zone are set at 60% of the $foEa_{max}$. The model uses linear interpolation to get values between the equatorial or

polarized auroral boundaries and the geomagnetic latitude of the $foEa_{max}$. FoEa, the interpolated value, is the auroral value of foE when no solar component is present (Auroral night line, Auroral sunrise, sunset). The height of maximum ionization for the auroral E layer is calculated as follows:

hmEa = 130.0 foEa $\leq$ 1.0

hmEa = 90.0 foEa $\geq$ 7.0

$$hmEa = 130.0 - \left[\frac{foEa - 1}{7.0 - 1.0}\right](130.0 - 90.0) \qquad 1.0 < foEa < 7.0$$

(3.17)

When there is an Auroral daytime point, the low and mid latitude value of the foE is used.

foEs = foE obtained from world maps

hmEs = hmE from low and mid latitude = 110 km

When both solar and auroral E components are present, the following rules are used to select the E layer critical frequency:

$foE = (foEs^4 + 1.5\ foEa^4)^{1/4}$ (hmEs - hmEa) $\leq$ 10.0

hmE = corresponding height (hmEa or hmEs) (hmEs - hmEa)>10.0

Auroral foF1

The auroral zone night time value of the F1 layer are set as follows:

foF1 = 0.2 MHz

hmF1 = 200.0 km

ymF1 = hmF1/4.0

The low and mid latitude values are used otherwise.

Auroral foF2 is calculated from the following equations (Tascione et.al. 1988)

$$foF2a = \sqrt{foF\,2_c^2 + 9.0\,\Delta N}$$

$$where\ foF2c = foF2\ evaluated\ by\ the\ coefficients$$

$$\Delta N = e^{-\frac{x_1^2}{2}}$$

$$X1 = \frac{(fa - lm)}{(fp - fa)}$$

$$where (fp - fa) = entire\ width\ of\ the\ auroral\ oval$$

(3.18)

λm = corrected geomagnetic latitude of interest

Φp = polward boundary of the oval

Φa = equatorward boundary of the oval

Φm = middle of the auroral oval

$X_1 = 2 * X_1$ if $\lambda m > \phi m$

HmF2 for the auroral oval is calculated the same as the low and mid latitude value.

3.5.3 Polar Cap

The polar E layer has a default set of parameters as follows:

foE = 0.6 Mhz

HmE = 120.0 km

ymE = 120.0/5.5 = 22 km

The polar F1 layer has a default set of parameters as follows:

foF1 = 0.2 Mhz

fmF1 = 200.00 km

ymF1 = 200.0/4.0 = 50.0 km

The polar F2 layer is calculated with the same formulas as the auroral zone.

3.5.4 Sub Auroral Trough

$$foF2 = foF2c$$
$$foF2 = (1 + \Delta N)$$

where foF2c is the foF2 from coefficients and where ΔN is the depletion region adjustment factor which is a function of both magnetic local time and geomagnetic activity. The following definition of ΔN is based upon Miller and Gibbs (1975):

$$\Delta N = T(1.0 + \cos[p(D + 11.0)/182.5])$$

where D is the Julian day and T is a complicated weighting factor dependent on local geomagnetic time, magnetic activity, and solar zenith angle.

$$T = T_1 \exp([\chi_1 - \chi_1^2] / 2.0) \exp[-1.0\ TPC^2 / 12.0]$$

where

$$\chi_1 = (\lambda_m - \Phi_A) / (3.7 + 1.3\ KP_{eff}$$
$$TPC = abs\ (TCGM - 3.0)$$

and

$$T_1 = 0.0 \quad \chi \leq 90 \text{ or } 6.0 < TCGM < 18.0$$
$$T_1 = -0.2 \quad \chi > 94.6 \text{ and } 18.0 \leq TCGM \leq 6.0$$
$$T_1 = [-0.2(\chi - 90)] / 4.6$$
$$90 \leq \chi \leq 94.6 \text{ and } 18.0 \leq TCGM \leq 6.0$$

In the above expressions, χ is the solar zenith angle, TCGM is the local geomagnetic time, λ_m is the corrected geomagnetic latitude of the point being considered, and ϕ_A is the geomagnetic latitude of the equatorward auroral boundary, Kp_{eff} is the effective Kp geomagnetic index.

The trough height values are calculated as follows. The low and mid latitude calculations are made at 4 points, centered on 0300 magnetic local time and the trough maximum. Calculation of hmF2 for the subauroral trough is

made for each point on the following grid:

Equatorial boundary of the auroral zone		Trough polward boundary
		Trough maximum
		Trough equatorial boundary
2000 MLT	0300 MLT	0700 MLT

At the trough maximum and 0300 magnetic local time (0300 MLT), the maximum height of the trough is set at 450 km. The value of hmF2 is calculated by interpolation in the above grid.

3.6 ELECTRON DENSITY PROFILE

For the generation of the electron density profile a single set of critical frequencies and associated parameters are chosen. Depending on the path length, a process of elimination is used to reduce up to 5 control points to 1 to 3 control points that best represent the ionosphere for that particular communications circuit. The ionospheric parameters (foE, hmE, ymE, foF1, hmF1.....etc) are then used to build an electron density profile at the control points based on the Chapman layer structure at the critical frequency and below, with exponential extensions on the topsides of the layers.

3.6.1 Control Point Selection

For each communication circuit, up to five geographic points are calculated along the circuit path. From these geographic locations, up to 3 control points are selected with ionospheric parameters assigned to each. When the ionospheric profile is generated, the layer parameters are selected from the values at the three control points.

Distance $\leq$ 2000 km 1 Control point

foF2	from path midpoint
fof1	from path midpoint
foE	from path midpoint

2000 km < Distance ≤ 4000 km 2 Control points

Control point 1

foF2	from path midpoint
foF1	1000 km from transmitter
foE	1000 from transmitter

Control point 2

foF2	path midpoint
foF1	1000 km from receiver
foE	1000 km from receiver

4000 < Distance ≤ 8000 km 3 Control points

Control point 1

foF2	2000 km from transmitter
foF1	1000 km from transmitter
foE	1000 km from transmitter

Control point 2

foF2	path midpoint
foF1	path midpoint
foE	path midpoint

Control point 3

foF2	2000 km from receiver
foF1	1000 km from receiver
foF2	1000 km from receiver

When circuit parameters that describe characteristics of the path are calculated, the profile is made up of the most pessimistic layer values, minimum foF2 or minimum foE when the FoF2 values are approximately equal.

3.6.2 Vertical Profile Generation

Once the layer characteristics are selected, then the profile based on the layer values (FoF2, FoF1, FoE, ...) is constructed. The initial step in the profiling routine is to extract the semi-thickness of the F2 and F1 (if χ

$\leq 105^{o}$) regions from the E-R model. The semi-thickness (ST) are then normalized by use of the empirical Wrobel function (Damon and Hartranft, 1970) as follows:

$$ST\ (F2) = ST\ (E\text{-}R) * W\ (hmF2_{ICED}) / W\ (hmF2_{E\text{-}R})$$

$$ST\ (F1) = ST\ (E\text{-}R) * W\ (hmF1_{ICED}) / W\ (hmF2_{E\text{-}R})$$

where

$$W(h) = 1n(h)/0.02186 - 203.447$$

is the expression for the Wrobel scale height and the subscripts indicate the source of the height of the maximum density value (E-R = Elkins-Rush 1973).

The profile is then constructed in the following manner:

(1) At and above the F2 layer peak, we closely follow the Elkins-Rush model with the exception of the modified F-region semi-thickness, and a modified top-side scale height using DMSP in-situ ion-electron measurements (if available).

(2) At and below the E layer peak, a Chapman layer with scale height of 16 km is used unless the F1 layer contribution at the E layer peak height exceeds the E layer density computed from either solar or particle ionizations. In this case, the E layer is disregarded and the F1 layer is extended downward.

(3) Between the F2 layer peak and the E layer height of maximum electron density, the modeling depends on whether or not the F1 layer is present.

(a) In the absence of the F1 layers, the electron density at any height is the sum of the density contributions from the E and F2 layers.

(b) When the sun is visible at F1 layer heights, the intermediate region is modeled by subtracting the F1 layer contribution at E and F2 layer heights from the maximum densities produced by the model for these two layers independently. The reduced E and F2 layer maximum densities are then used in the Chapman function representing each layer. Finally, the total electron density at any level is the sum of the density contributions from the F1 layer and the modified E and F2 layers. In this procedure, the Chapman scale height of the F2 layer is decreased, if necessary, to insure that the F1 layer peak falls at least two (F2) scale heights below the F2 peak. The above technique,

then allows the F2 and E layer peak densities to be modeled exactly and generally results in an F1 density within 5 percent of the target value.

3.7 VIRTUAL HEIGHT RAY PATH AND AREA COVERAGE MODEL FOR SINGLE HOP PROPAGATION

This section describes a simple computation method for obtaining all the single-hop ray paths through an ionosphere described by an electron density profile. It uses the classical relationships between the virtual-height ionograms and the oblique path (however, Martyn's equivalence theorem is used in a "corrected" form as described in Section 3.7.4). First, the ionogram is obtained using numerical integration techniques. Then reflectrices are obtained as single table entering all ray-path information. Finally, the correction to Martyn's theorem and a table look up and interpolation procedure are used to find the ray sets which describe the propagation for a particular operating frequency.

3.7.1 Virtual Height Ionograms

Virtual heights for the ordinary trace are found from the electron density profile by numerically integrating the equation.

$$h'(f_v) = h_0 + l\int_{h_0}^{h_r} m'(h, f_v)\, dh$$

where

$$m'(h, f_v) = \left[1 - \frac{f_N^2(h)}{f_v^2}\right]^{-1/2}$$

(3.19)

f_v is a selected vertical sounding frequency;
h_o is the lowest true height of the profile, i.e., 70 km;
h' is the virtual height of the profile;
h_r is the true height corresponding to f_v;
h is the true height of reflection;
μ' is the group index of refraction;

f_N is the plasma frequency.

The area is found using a Gaussian integration technique (see Figure 1). The effect of the cusp at h_r can be lessened by using a nonlinear transformation from
the interval $[h_o, h_r]$, to [-1, 1]. The transformation and integration equations are:

h_j = true height corresponding to (w_j, X_j);
X_j = Gaussian abscissa;
w_j = Gaussian weight;
N = number of Gaussian terms (at least 40) for electron density profiles described in Section 3.6.2.

A forty-point Gaussian integration was found to be adequate when the electron density profile was sampled at true height intervals of 4 km and the vertical sounding frequencies were selected at intervals of 0.2 MHz.

3.7.2 Skywave Propagation

Skywave radio propagation paths may be described by a set of parameters known as raysets (Croft, 1967). For most HF communication applications, this consists of operating frequency, takeoff angle, virtual height of reflection, true height of reflection, and ground distance. The basic inputs are true and virtual heights as a function of critical-incidence frequency.

The ray paths are calculated using the following simplifying assumptions:

1. Horizontal and azimuthal variations in the ionospheric electron density profiles are negligible for each hop (on a multi-hop path, different sample area are used).
2. The magnetic field may be ignored.
3. The ionosphere is spherically symmetrical to the earth.

With these simplifications, the equivalence between a given frequency on an oblique path (f_{ob}) and a vertical incidence frequency (f_v) with same vertical height specified by Snell's law is

$$f_{ob} = f_v \sec\theta_t \qquad (3.20)$$

where

θ_t is the angle between the apparent ray path and the normal to the earth at the true height of reflection.

By simple geometry, the virtual height of the oblique path is related to the takeoff angle Δ by (see Figure 2).

$$a \cos \Delta = (a + h'_{ob}) \sin \Phi \qquad (3.21)$$

where

Δ = takeoff angle of the ray,

a = earth's radius,

h'_{ob} = virtual height of the oblique path,

Φ = is the angle between the virtual ray and the normal to the earth at h'_{ob}.

Martyn's theorem for a plane ionosphere specified the ray path by the equality of the virtual height of the oblique path, with the virtual height of the ionogram at the equivalent frequency f_v. For a curved ionosphere, this leads to a consistent error at higher frequencies for thicker layers. The Breit and Tuve theorem states that the time taken to transverse the actual path is the same as that which would be taken to transverse the equivalent path in free space. Both theorems are corrected in the following model by an empirically derived correction factor which depends only on the electron density profile and the curvature of the ionosphere:

$$h_{o'b} = h_{v'} + \left(\frac{f_{ob}^2 - f_v^2}{foF} 2^2 \right) \left[h \left(\frac{h_{v'} - h}{a} \right) + 2(a+h) \left(\frac{h_{v'} - h}{a} \right)^2 \right] \qquad (3.22)$$

where

foF2 is the F2 critical frequency,

h'_v is the virtual height corresponding to f_v,

h is the true height of reflection.

This correction has errors of less than one percent as compared with the distances calculated by a ray-trace program based on Haselgrove's equation method (Haselgrove, 1954; Finney, 1963). This is described in more detail in

the following section.

The model uses equations 3.20 and 3.21 to generate Table 1. The first row is the vertical-incidence frequency in megahertz. The second row is the true height of reflection, h; the third row is the virtual height of reflection, h'; and the rows following are the equivalent oblique operating frequencies of the transmitter for ray paths with corresponding takeoff angles; e.g., the row after 0.0 is for ray paths with a takeoff angle of 0^{o}. When the information contained in Table 1 is plotted in constant frequency contours of virtual reflection height and distances as in Figure 3, the displayed contours are called reflectrices (Lejay and Lepechinsky, 1950). At each given operating frequency, the area coverage is found by interpolating in Table 1 for the desired ray paths. This procedure yields the desired reflectrix for the given frequency in the form of a table of raysets (Table 2). Calculations are not necessary at each frequency as all the desired information is contained in Table 1. For two-hop modes, a table of reflectrix information (as in Table 1) is generated for the second-hop sample area, and at the given operating frequency, a table of rayset information is generated (as in Table 2). The two-hop modes are found by matching the takeoff angle of the second hop with the arrival angle of the first hop. Note that there has been no mention of individual layers (E, F1, or F2) since the electron density profile was generated. The ionosphere is treated as a single region by the program, and all possible mode combinations are generated. In order to keep the traditional layer nomenclature, the ray paths are named according to where their equivalent vertical frequencies lie (e.g., below foE); thus the modes may be E-E, F2-F2, or E-F2 according to the label of each hop. Since the sporadic-E modes are assumed to exist with some degree of probability with reflection at a constant height, the rayset information is the same for each operating frequency and there is no need to generate the equivalent of Table 1 for the Es mode.

Table 1 Showing the Relationship Between Vertical Incidence Data (Ionogram) and Oblique Propagation (Reflectrix)

IONOGRAM AND REFLECTRIX

FVERT	.01	.91	1.82	2.72	2.83	2.95	3.06	3.17	3.29	3.40	3.40	3.51	3.62	3.73	3.84
HTRUE	70.0	74.2	89.0	98.0	99.0	100.0	101.3	102.9	105.0	110.0	153.8	155.0	156.7	158.5	160.4
HPRIM	70.0	83.9	103.0	114.0	114.6	116.3	119.6	124.4	132.1	175.7	328.4	241.0	231.3	226.7	226.5

ANGLES	OBLIQUE FREQUENCIES kHz														
0.0	68	6036	10983	15684	16257	16822	17358	17867	18325	18532	15760	16204	16630	17046	17454
.5	67	6026	10968	15665	16238	16802	17337	17847	18304	18512	15748	16192	16617	17035	17440
1.0	67	5997	10924	15608	16179	16741	17276	17784	18242	18452	15711	16154	16579	16997	17402
2.0	66	5885	10753	15385	15950	16507	17039	17542	17998	18216	15567	16007	16430	16846	17249
3.0	64	5711	10484	15034	15590	16138	16661	17160	17613	17844	15336	15772	16191	16603	17003
4.0	61	5492	10141	14582	15125	15661	16174	16666	17115	17359	15029	15459	15873	16280	16676
5.0	58	5245	9746	14057	14585	15106	15608	16089	16532	16791	14661	15083	15491	15892	16283
6.0	55	4984	9321	13487	13998	14504	14991	15461	15897	16168	14246	14660	15060	15454	15839
8.0	49	4466	8452	12305	12779	13249	13706	14148	14565	14856	13335	13729	14111	14489	14858
10.0	44	3991	7030	11167	11604	12039	12461	12875	13268	13567	12391	12762	13125	13483	13825

12.0	39	3578	6895	10136	10538	10937	11328	11712	12081	12378	11478	11826	12168	12506	12840
14.0	35	3227	6257	9230	9599	9966	10327	10683	11028	11319	10626	10955	11276	11595	11909
16.0	32	2930	5709	8444	8784	9123	9457	9787	10107	10390	9855	10164	10465	10765	11061
18.0	29	2679	5239	7765	8079	8393	8703	9010	9310	9580	9166	9453	9736	10018	10297
20.0	27	2465	4835	7179	7471	7762	8051	8338	8619	8876	8562	8821	9088	9353	9616
22.0	25	2283	4488	6672	6944	7216	7486	7754	8018	8263	8006	8260	8511	8761	9010
24.0	23	2126	4186	6231	6486	6741	6994	7246	7494	7728	7523	7762	7999	8236	8471
26.0	21	1989	3924	5846	6086	6326	6564	6801	7036	7258	7093	7320	7545	7769	7992
28.0	20	1871	3694	5508	5734	5961	6186	6410	6633	6845	6711	6926	7140	7353	7565
30.0	19	1766	3492	5210	5424	5639	5852	6065	6276	6480	6370	6574	6778	6981	7183
32.0	18	1675	3314	4945	5150	5354	5557	5759	5961	6155	6065	6260	6454	6648	6842
34.0	17	1593	3155	4710	4905	5100	5294	5487	5679	5866	5791	5978	6164	6350	6535
36.0	16	1521	3013	4501	4687	4873	5058	5244	5428	5607	5545	5724	5903	6081	6259
38.0	15	1456	2886	4313	4491	4670	4848	5025	5202	5375	5323	5495	5667	5839	6010
40.0	15	1398	2772	4143	4315	4487	4658	4829	4999	5166	5123	5289	5454	5619	5784

42.0	14	1346	2670	3991	4157	4322	4487	4652	4816	4978	4941	5101	5261	5421	5580
44.0	14	1298	2577	3853	4013	4173	4333	4492	4651	4608	4777	4932	5086	5241	5395
46.0	13	1256	2493	3729	3884	4038	4193	4347	4501	4653	4627	4777	4926	5077	5227
48.0	13	1217	2417	3616	3766	3916	4066	4216	4365	4513	4491	4637	4783	4928	5074
50.0	12	1182	2348	3513	3659	3805	3951	4096	4242	4386	4367	4509	4651	4793	4934
52.0	12	1151	2286	3420	3562	3704	3846	3988	4130	4270	4255	4393	4531	4669	4807
54.0	12	1122	2229	3335	3474	3613	3751	3889	4028	4165	4152	4287	4422	4557	4692
56.0	12	1095	2177	3258	3394	3529	3665	3800	3935	4069	4058	4190	4322	4454	4586
58.0	11	1072	2130	3188	3321	3453	3586	3718	3851	3982	3973	4103	4232	4361	4490
60.0	11	1050	2088	3125	3255	3385	3515	3644	3774	3908	3696	4023	4150	4276	4403
65.0	11	1005	1998	2991	3115	3240	3364	3489	3613	3737	3733	3854	3976	4098	4219
70.0	10	970	1929	2888	3009	3129	3249	3359	3489	3609	3607	3725	3842	3960	4078
75.0	10	944	1878	2812	2930	3047	3164	3281	3398	3515	3514	3629	3743	3858	3973
80.0	10	927	1843	2760	2875	2990	3105	3220	3335	3450	3450	3562	3675	3788	3900
85.0	10	916	1823	2730	2843	2957	3071	3184	3298	3412	3412	3524	3635	3746	3858
90.0	10	9l3	l8l6	2720	2833	2946	3059	3173	3286	3399	3400	3511	3622	3733	3844

Table 2. Rayset Table for 10 MHz. Great-Circle Distance (km), Vertical Angle (Degrees), Virtual and True Reflection Heights (km), Propagation Mode, and Equivalent Vertical Incidence Frequency (f_v in MHz)

RAYSET FOR FREQUENCY =10.00 MHz

DISTANCE	ANGLE	VIRTUAL	TRUE	MODE	FV
2240.69	0.00	99.81	86.03	E	1.64
2132.85	.50	99.85	86.07	E	1.64
2031.62	1.00	100.03	86,19	E	1.65
1848.52	2.00	100.66	86.68	E	1.68
1689.82	3.00	101.70	87.46	E	1.73
1553.09	4.00	103.08	88.51	E	1.79
1431.40	5.00	104.33	89.49	E	1.87
1323.49	6.00	105.49	90.43	E	1.96
1147.44	8.00	108.15	92.59	E	2.18
1012.11	10.00	111.13	95.02	E	2.42
906.11	12.00	114.34	97.62	E	2.68
819.51	14.00	117.39	100.15	E	2.96
1024.54	16.93	181.35	109.96	E	3.40
1817.87	16.93	359.68	153.64	1	3.40
1213.47	18.00	234.01	158.34	1	3.73
1121.66	20.00	237.04	163.87	1	4.01
1194.88	22.00	280.89	174.09	1	4.31
1496.14	22.52	374.11	182.41	1	4.40
2184.89	22.52	595.08	210.45	2	4.40
1349.37	24.00	354.18	215.75	2	4.68
1209.20	26.00	340.38	221.60	2	4.96
1133.73	28.00	343.83	228.35	2	5.23
1094.45	30.00	358.10	236.32	2	5.50
1084.19	32.00	383.12	246.06	2	5.77
1127.25	34.00	432.03	259.43	2	6.05
1942.44	35.70	874.76	290.49	2	6.30

3.7.3 Corrected Martyn's Theorem

The model derives the rays as described above in the following manner: first the virtual height of reflections are derived by numerical integration (40 point Gaussian quadrature)

$$h'(f_v) = \int_0^{h_r} m'(f_v, h)\, dh \qquad (3.23)$$

h_r is the true height of reflection and $\mu'(f_v, h)$ is the group index of refraction.

For each radiation (takeoff) angle Δ, Snell's law is used to find the oblique frequency corresponding to f_v, the vertical sounding frequency:

$$f_{ob} = f_v \sec \Phi$$
$$\sin \Phi = \cos \Delta / (1 + h'/a).$$

Then the distance is found using Martyn's theorem for equivalence of oblique and vertical heights of reflectivity (first source of error as it is valid only for a "flat" ionosphere). See figure 2.

$$D = 2a (\pi - \Delta - \Phi')$$

where

$$\sin \Phi' = \cos \Delta / (1 + h'/a)$$

h' is the virtual height corresponding to h_r as derived above.

Finally the group path is found using the law of Breit and Tuve (second source of error as it is valid only for a "flat" ionosphere):

$$P' = 2a \cos (\Phi' + \Delta) / \sin \Phi'.$$

To compensate for the above errors, the following correction was used.

$$h_{o'b} = h_{v'} + \left(\frac{f_{ob}}{f_c} \right)^2 (m_r^2) \left[h \left(\frac{h_{v'} - h}{a} \right) + 2(a + h) \left(\frac{h_{v'} - h}{a} \right)^2 \right]$$

where

$$m_r^2 = 1 - \frac{f_n^2}{f_{ob}^2} \quad with \quad f_N = f_v$$

(3.24)

3.8 PROBABILITY OF SKY-WAVE PROPAGATION

Since the MUF calculated is based upon median values of the ionospheric characteristics, the probability of a sky-wave path for this frequency is assumed to be 50 percent. The frequency that would have a 90 percent probability of propagating (FOT) and the frequency which has 10 percent probability (HPF) are obtained by multiplying the MUF by the factors given in table 3.

The values in table 3 were derived from a study (R.M. Davis and N.L. Groome, 1964, private communication) of the distribution of daily values of MUF about their monthly median. The data used in this study were values of the standard MUF, which is the product of the foF2 and M(3000)F2 factors scaled from vertical incidence ionograms. Data from 13 stations located at geomagnetic latitudes from 71^{o}S to 88^{o}N were analyzed. The temporal variations of the MUF distribution were determined by considering observations at all hours of the day, each month of the year, and periods representing low, medium, and high solar activity. Values were derived for the ratios of upper and lower decile MUFs to median MUF for a given season, a given solar activity, 4-hour local time blocks, and each 10^{o} of geographic latitude from 10^{o} to 80^{o}, north or south.

The values in table 3 reflect some general trends. The MUF distribution is wider at night than during the day, and wider at low latitudes than high latitudes in daytime. Also, in daytime, the distribution is wider in summer than winter, except at high latitudes where the reverse is true. Dependence on solar activity is weak, but during daytime hours the difference between the decile ratios generally seems to increase with solar activity at latitudes above 40^{o}. The study by Davis and Groome (1964, private communication) indicates that the distribution is mostly dependent on foF2, not on the M(3000)F2 factor; therefore, the distributions are assumed valid for any oblique path.

TABLE 3. FACTORS FOR CALCULATING FOT AND HPF FROM MUF LOCAL TIME

N. Hemisphere (Nov., Dec., Jan., Feb.)

Winter

{ S. Hemisphere (May, June, July, Aug.)

Low (0-50) Sunspot Number

Geo.	22-02		02-06		06-10		10-14		14-18		18-22		Geo.
Lat.	Fu	Fl	Fu	Fl	Fu	Fl	Fu	Fl	Fu	Fl	Fu	Fl	Lat.
> 75	1.44	.60	1.34	.65	1.45	.69	1.32	.72	1.33	.68	1.40	.67	> 75
65-75	1.37	.68	1.29	.71	1.38	.75	1.23	.76	1.24	.75	1.35	.70	65-75
55-65	1.30	.74	1.24	.76	1.27	.80	1.15	.80	1.17	.82	1.30	.73	55-65
45-55	1.25	.79	1.21	.78	1.16	.83	1.12	.85	1.12	.84	1.25	.76	45-55
35-45	1.23	.81	1.20	.79	1.13	.85	1.11	.87	1.11	.89	1.23	.77	35-45
25-35	1.28	.81	1.30	.74	1.15	.86	1.17	.82	1.15	.85	1.28	.78	25-35
15-25	1.34	.78	1.37	.67	1.19	.87	1.20	.75	1.24	.77	1.32	.79	15-25
≤ 15	1.27	.71	1.38	.70	1.18	.88	1.15	.86	1.14	.87	1.20	.79	≤ 15

Medium (50-100) Sunspot Number

Geo.	22-02		02-06		06-10		10-14		14-18		18-22		Geo.
Lat.	Fu	Fl	Fu	Fl	Fu	Fl	Fu	Fl	Fu	Fl	Fu	Fl	Lat.
> 75	1.45	.76	1.39	.78	1.44	.68	1.40	.67	1.33	.62	1.45	.70	> 75
65-75	1.39	.79	1.31	.81	1.37	.74	1.32	.70	1.29	.73	1.41	.73	65-75
55-65	1.33	.82	1.24	.83	1.25	.79	1.21	.75	1.22	.80	1.33	.76	55-65
45-55	1.30	.84	1.19	.82	1.14	.83	1.15	.81	1.16	.84	1.29	.78	45-55
35-45	1.27	.83	1.17	.81	1.12	.85	1.14	.86	1.14	.86	1.28	.79	35-45
25-35	1.30	.78	1.31	.76	1.16	.85	1.18	.85	1.18	.85	1.32	.78	25-35
15-25	1.33	.74	1.38	.71	1.17	.85	1.22	.83	1.26	.82	1.40	.76	15-25
≤ 15	1.21	.77	1.26	.69	1.14	.87	1.13	.86	1.15	.85	1.23	.78	≤ 15

High (>100) Sunspot Number

Geo.	22-02		02-06		06-10		10-14		14-18		18-22		Geo.
Lat.	Fu	Fl	Fu	Fl	Fu	Fl	Fu	Fl	Fu	Fl	Fu	Fl	Lat.
> 75	1.36	.62	1.27	.70	1.41	.74	1.42	.67	1.40	.64	1.43	.73	> 75
65-75	1.31	.69	1.25	.74	1.34	.77	1.30	.72	1.16	.72	1.34	.78	65-75
55-65	1.26	.77	1.23	.78	1.24	.81	1.18	.80	1.11	.79	1.26	.82	55-65
45-55	1.19	.83	1.19	.80	1.16	.84	1.11	.87	1.09	.84	1.20	.86	45-55
35-45	1.15	.86	1.14	.81	1.13	.87	1.09	.90	1.09	.87	1.14	.87	35-45
25-35	1.22	.83	1.26	.76	1.12	.89	1.09	.90	1.11	.88	1.13	.86	25-35
15-25	1.32	.78	1.35	.70	1.12	.89	1.12	.89	1.14	.89	1.20	.83	15-25
≤ 15	1.18	.83	1.25	.76	1.14	.89	1.13	.90	1.15	.89	1.20	.84	≤ 15

TABLE 3. FACTORS FOR CALCULATING FOT AND HPF FROM MUF LOCAL TIME (CONT.)

Equinox (Mar., Apr., Sept., Oct.)

Low (0-50) Sunspot Number

Geo.	22-02		02-06		06-10		10-14		14-18		18-22		Geo.
Lat.	Fu	Fl	Fu	Fl	Fu	Fl	Fu	Fl	Fu	Fl	Fu	Fl	Lat.
> 75	1.42	.67	1.32	.72	1.29	.74	1.26	.73	1.33	.80	1.48	.65	> 75
65-75	1.38	.70	1.25	.75	1.25	.76	1.23	.74	1.26	.82	1.40	.69	65-75
55-65	1.32	.73	1.21	.78	1.22	.80	1.20	.75	1.20	.81	1.31	.73	55-65
45-55	1.26	.75	1.19	.80	1.20	.81	1.18	.76	1.16	.81	1.26	.76	45-55
35-45	1.22	.77	1.20	.81	1.19	.81	1.16	.77	1.16	.80	1.25	.78	35-45
25-35	1.22	.78	1.26	.80	1.18	.82	1.15	.78	1.16	.81	1.28	.74	25-35
15-25	1.30	.77	1.32	.75	1.16	.83	1.14	.81	1.18	.83	1.33	.69	15-25
≤ 15	1.23	.76	1.40	.66	1.13	.86	1.13	.89	1.19	.86	1.16	.75	≤ 15

Medium (50-100) Sunspot Number

Geo.	22-02		02-06		06-10		10-14		14-18		18-22		Geo.
Lat.	Fu	Fl	Fu	Fl	Fu	Fl	Fu	Fl	Fu	Fl	Fu	Fl	Lat.
> 75	1.45	.64	1.31	.61	1.27	.73	1.28	.74	1.30	.74	1.47	.67	> 75
65-75	1.41	.68	1.22	.71	1.23	.77	1.26	.74	1.26	.78	1.38	.70	65-75
55-65	1.35	.70	1.17	.75	1.20	.80	1.23	.72	1.18	.78	1.29	.73	55-65
45-55	1.28	.73	1.15	.77	1.17	.81	1.21	.74	1.13	.76	1.20	.75	45-55
35-45	1.22	.75	1.16	.78	1.16	.82	1.18	.78	1.12	.76	1.17	.76	35-45
25-35	1.22	.77	1.22	.76	1.15	.82	1.17	.83	1.14	.78	1.23	.72	25-35
15-25	1.32	.75	1.30	.73	1.13	.84	1.15	.87	1.17	.81	1.37	.69	15-25
≤ 15	1.18	.79	1.39	.68	1.11	.86	1.13	.89	1.20	.84	1.23	.80	≤ 15

High (>100) Sunspot Number

Geo.	22-02		02-06		06-10		10-14		14-18		18-22		Geo.
Lat.	Fu	Fl	Fu	Fl	Fu	Fl	Fu	Fl	Fu	Fl	Fu	Fl	Lat.
> 75	1.46	.66	1.37	.67	1.35	.75	1.40	.66	1.38	.70	1.46	.72	> 75
65-75	1.42	.67	1.31	.71	1.30	.73	1.31	.70	1.33	.70	1.37	.72	65-75
55-65	1.30	.69	1.25	.75	1.27	.71	1.24	.71	1.25	.71	1.24	.72	55-65
45-55	1.18	.73	1.20	.78	1.25	.70	1.20	.72	1.16	.74	1.17	.73	45-55
35-45	1.15	.79	1.16	.82	1.17	.75	1.16	.78	1.12	.80	1.14	.82	35-45
25-35	1.25	.81	1.18	.82	1.10	.87	1.10	.87	1.11	.87	1.15	.86	25-35
15-25	1.31	.81	1.32	.77	1.11	.89	1.11	.92	1.12	.90	1.20	.85	15-25
≤ 15	1.21	.80	1.23	.79	1.09	.86	1.20	.90	1.14	.90	1.23	.82	≤ 15

TABLE 3. FACTORS FOR CALCULATING FOT AND HPF FROM MUF LOCAL TIME (CONT.)

N. Hemisphere (May., June., July., Aug.)

Summer

{ S. Hemisphere (Nov., Dec., Jan., Feb.)

Low (0-50) Sunspot Number

Geo.	22-02		02-06		06-10		10-14		14-18		18-22		Geo.
Lat.	Fu	Fl	Fu	Fl	Fu	Fl	Fu	Fl	Fu	Fl	Fu	Fl	Lat.
> 75	1.26	.68	1.24	.79	1.15	.84	1.17	.87	1.21	.85	1.22	.76	> 75
65-75	1.22	.70	1.18	.81	1.14	.83	1.15	.86	1.16	.86	1.18	.77	65-75
55-65	1.18	.72	1.17	.84	1.14	.83	1.15	.84	1.14	.86	1.15	.81	55-65
45-55	1.17	.75	1.20	.85	1.15	.82	1.16	.83	1.14	.85	1.15	.84	45-55
35-45	1.17	.79	1.25	.85	1.17	.80	1.17	.82	1.15	.83	1.16	.85	35-45
25-35	1.18	.79	1.30	.82	1.17	.78	1.20	.80	1.19	.81	1.20	.80	25-35
15-25	1.20	.77	1.34	.78	1.14	.77	1.24	.79	1.22	.79	1.23	.73	15-25
≤ 15	1.20	.74	1.37	.75	1.12	.80	1.30	.83	1.27	.82	1.20	.69	≤ 15

Medium (50-100) Sunspot Number

Geo.	22-02		02-06		06-10		10-14		14-18		18-22		Geo.
Lat.	Fu	Fl	Fu	Fl	Fu	Fl	Fu	Fl	Fu	Fl	Fu	Fl	Lat.
> 75	1.27	.82	1.23	.80	1.20	.82	1.18	.85	1.25	.80	1.23	.79	> 75
65-75	1.23	.83	1.19	.82	1.19	.79	1.17	.82	1.17	.82	1.19	.82	65-75
55-65	1.20	.83	1.18	.82	1.19	.77	1.17	.79	1.14	.82	1.17	.83	55-65
45-55	1.17	.81	1.19	.81	1.21	.76	1.17	.77	1.15	.81	1.16	.82	45-55
35-45	1.17	.78	1.22	.78	1.23	.75	1.18	.78	1.17	.78	1.17	.78	35-45
25-35	1.20	.77	1.30	.73	1.22	.75	1.19	.79	1.19	.77	1.18	.74	25-35
15-25	1.26	.77	1.38	.69	1.17	.78	1.23	.82	1.23	.78	1.28	.73	15-25
≤ 15	1.26	.79	1.44	.63	1.11	.84	1.28	.85	1.28	.81	1.22	.77	≤ 15

High (>100) Sunspot Number

Geo.	22-02		02-06		06-10		10-14		14-18		18-22		Geo.
Lat.	Fu	Fl	Fu	Fl	Fu	Fl	Fu	Fl	Fu	Fl	Fu	Fl	Lat.
> 75	1.30	.73	1.27	.74	1.17	.82	1.15	.83	1.23	.79	1.24	.75	> 75
65-75	1.22	.75	1.22	.75	1.20	.77	1.18	.80	1.21	.80	1.23	.77	65-75
55-65	1.16	.77	1.18	.76	1.26	.74	1.21	.77	1.19	.80	1.21	.80	55-65
45-55	1.14	.79	1.15	.76	1.30	.73	1.26	.75	1.19	.80	1.18	.84	45-55
35-45	1.14	.80	1.14	.76	1.30	.75	1.27	.75	1.19	.79	1.16	.84	35-45
25-35	1.16	.81	1.15	.76	1.25	.82	1.20	.81	1.17	.79	1.15	.83	25-35
15-25	1.21	.81	1.22	.77	1.18	.85	1.15	.86	1.18	.81	1.19	.80	15-25
≤ 15	1.25	.80	1.21	.79	1.13	.86	1.17	.89	1.22	.85	1.23	.78	≤ 15

.1 Based on the values in table 3, the probability of ionospheric support at a given frequency is determined by evaluating the Gaussian probability distribution function.

The standard deviation is first evaluated as follows:

$$s = \frac{MUF - F(I,J,K)KMUF}{1.28}$$

where F(I,J,K) are the multiplying factors from table 3 and I,J,K are indexs that represent latitude, low or high sunspot number, and time of day.

Then the probability that the operating frequency (F) is greater than the FOT, MUF, or HPF for a given layer using the MUF distribution is

$$P(\frac{x-m}{s}) = P(\frac{F-MUF}{s}) = \frac{1}{2p}\int_{-\infty}^{\frac{F-MUF}{s}} d\frac{-t^2}{2}\,dt$$

The E layer is stable and very predictable; therefore, if the E layer supports propagation, it is assumed to have a probability of 0.99.

3.9 PROBABILITY OF SPORADIC-E PROPAGATION

The program contains an option for considering sporadic-E propagation in the system performance predictions. Sporadic-E propagation is not considered when calculating the MUF, because the median value of foEs does not represent a true critical frequency and is used simply to estimate the probability of occurrence of sporadic E. It is only considered when regular E-layer propagation is not possible.

The median and upper and lower decile values of foEs are obtained from the numerical coefficients (see sec. 2.4), and converted into values for the oblique path by the secant law relationship. The multiplicative factor, sec Φ, is computed as follows:

$$\sec f = \frac{1}{\cos(\frac{p}{2} - \frac{d}{2} - b)}$$

(3.35)

where

d/2 = half the great-circle path length in radians,

β = takeoff angle obtained from (3.17), with h' = 110 km.

The probability of sporadic-E propagation is then calculated for the operating frequency from these median and decile values using the normal probability function. As discussed in section 3.4, no additional loss is determined for the partial transparency of the E_s layer to radio waves.

3.10 Calculation of Mixed Modes

For path lengths equal to or greater than 3000 km, two N-type mixed modes of propagation are considered. This type consists of one E or E_s hop, with the remainder of the propagation path via the F layer. If E-layer propagation is not possible, the probability of E_s propagation is determined and combined with the probability of subsequent F-layer propagation. Normally, a mixed mode is not the most reliable mode.

4. NOISE PARAMETERS

The probability of successful transmission depends on the probability that the available signal-to-noise ratio at the receiving location is above a specified level. This level is the one required for a specified grade of service (see sec. 7) in the presence of noise, but in the absence of any other unwanted signals. The three major types of external noise with which the HF signal must compete are galactic, atmospheric, and man-made. In general, these noise sources have spectral energy distributions that vary more or less uniformly over the entire high frequency range. All values of noise are considered representative of those that would be expected with a short vertical lossless receiving antenna. No allowance is made in the program to account for the directional and polarization properties of other types of receiving antennas that could alter the available signal-to-noise ratio.

4.1 GALACTIC NOISE

Estimates of galactic (cosmic) noise are obtained from measurements (Spaulding and Disney (1974) CCIR Report 258-4(1982)).

The median galactic noise is represented by

$$N_g = 52.0 + 23 \log_{10} (f) - 204 \text{ dBW} \qquad (4.1)$$

where

$10 \log_{10} kTo = 204$ db

k = (Boltzmann;s constant) $1.38 * 10^{-23}$ Joules/degree Kelvin

To = Reference temperature 288^{o} K

N_g = expected median value of the galactic noise power in decibels relative to 1 W in a 1 Hz bandwidth,

f = frequency in megahertz.

The temporal variation is estimated at ±2 dB (CCIR, 1982), and values represent the upper limit of galactic noise. Ionospheric shielding of galactic noise is determined by evaluating the F-layer critical frequency above the receiving location. Directional properties of the receiving antenna are not considered. Estimates of the uncertainty in predicting the median and deciles are 0.5 dB and 0.2 dB, respectively.

4.2 ATMOSPHERIC NOISE

In the HF band, N_a, the atmospheric noise, is the most erratic of the three major types of noise. It is generally characterized by short pulses with random recurrence superimposed upon a background of random noise (Spaulding and Disney (1974)). Averaging these short pulses of noise power over several minutes yields average values that are nearly constant during a given hour. The variations seldom exceed ± 2 dB, except during sunrise or sunset periods and when local thunderstorms are present. Worldwide maps published in CCIR Report 322-3, representing the median of hourly medians of atmospheric noise at 1 MHz within 4-hour time blocks for the four (3-month) seasons of the year, are used as the basis for estimating this noise at any given receiving locations. Levels of atmospheric noise for other frequencies and its associated distribution about the median are available for each time block and season.

The maps in CCIR Report 322-3 were used to generate, by means of a least squares fit based on Fourier analysis, numerical coefficients representing the worldwide distribution of atmospheric noise (Spaulding and Washburn, 1985) as a function of geographic location. The curves of frequency dependence and variability of the radio noise were generated from a power series of least squares fit. The numerical maps and complete listings of the numerical coefficients used in the prediction program are given in NTIA Report 85-173 (Spaulding and Washburn).

The numerical coefficients in latitude, longitude, and local mean time at the receiving location give the median atmospheric noise power in decibels above k T_o b, at 1 MHz for each time block and season. The value of k (Boltzmann's constant) is 1.38×10^{-23} Joules per degree Kelvin, the reference temperature is 288°K, $10 \log_{10} kT_o$ = 204 dB below one joule, and b is the bandwidth in Hz. Noise values for other frequencies and their distributions are evaluated from numerical arrays derived from the frequency curves for each time block and season.

4.3 MAN-MADE NOISE

At certain receiving locations, unintended man-made radio noise may be the predominant external noise with which the communication system must compete. It may arise from any number of sources, such as power lines, industrial machinery, ignition systems, etc., and thus have wide geographic and short-term variations.

Information for deriving specific man-made noise levels as a function of geographic location and time is insufficient, but from the limited observations available, it is possible to express typical levels of unintended radiation (JTAC, 1968).

Four models are used to designate the median level of man-made noise, all based on the following equation:

$$N_m = c + d \log_{10} f - 204 \text{ dBW} \qquad (4.2)$$

where

N_m = man-made noise power in decibels below 1 W in a 1 Hz bandwidth,

f = frequency in megahertz,

c,d = constants derived from measurements and given below.

Values of c,d for each of the four models, are given below.

Values of Parameters for the Man-Made Noise Models

Environmental category	c	d
Business (curve A)	76.8	27.7
Residential (curve B)	72.5	27.7
Rural (curve C)	67.2	27.7
Quiet rural (curve D)	53.6	28.6
Galactic noise (curve E)	52.0	23.0

Urban location is defined as one within the industrial-business area of large cities, residential is one near a large city or within a small town, and rural location is one well removed from all populated areas and chosen to be as free as possible of man-made noise. The upper and lower decile values of N_m are 9.7 dB and 7.0 dB. Estimates of the uncertainty in predicting the median and deciles are 5.4 db and 1.5 db respectively.

When the user inserts his own value of man-made noise power in decibels below 1 watt in a 1 Hz bandwidth at 3 MHz (N_{user}), the suburban noise curve is used. In the program, the suburban curve is shifted vertically and includes the noise value at 3 MHz specified by the user.

4.4 COMBINATION OF NOISE

The three basic noise sources, man-made, galactic, and atmospheric noise, are independent of each other and must be combined by a statistically accurate method in order to represent the overall noise level at the site of interest. The current noise distributions are considered log normal and the method used to combine them is to determine the log normal distributions that best approximate the true distribution of the sum. The method used is a rather complex mathematical process. For specific information refer to an updated noise model for use in IONCAP (Spaulding, A.D. and Stewart, F.G. (1987).

Three major changes have been made with the new noise model: The replacement of the world wide atmospheric radio noise estimates with the current, much improved estimates of CCIR report 322-3; the replacement of the man-made noise estimates with the much more modern estimates of CCIR Report 258-4; and the overall distribution and its statistical variations have been updated.

5. IONOSPHERIC LOSS MODEL

This section describes the equations used to calculate ionospheric losses for a single-hop mode. The model is intended to cover the frequency band from 3 to 30 MHz. All modes which result from a complete electron density profile are covered, as well as sporadic-E modes. Lower decile, median, and upper decile values of field strength (signal or signal-to-noise ratio) can be determined by the methods described. The theoretical background and method of measurements are given in the manual on Ionospheric Absorption Measurements (Rawer, 1976). The equations described below are intended to be used on a worldwide basis, and are limited by the available worldwide prediction data base.

The equations are based on the CCIR 252-2 (1970) loss equation using a philosophy that modifications are made only when measured values demand a change. The CCIR loss equation was primarily derived from F2 low-angle modes with operating frequencies not greater than the FOT. For these conditions, there is no need to modify the equation. For E-layer low-angle modes, two modifications were necessary. A correction factor to account for less E-Layer bending was added [Equation (5.8)]. Since an arbitrary electron density profile can be used, the true height of reflection may be written into the D-layer absorbing region, resulting in lower absorption. This has been accounted for by modifying the collision frequency factor in the denominator [Equation (5.10)]. In addition to the D-region losses due to absorption, there may be losses at the area of reflection if the ionization of the region is insufficient to reflect all the radio energy. This loss increases as frequency increases, starts to be significant as the frequency nears the MUF, and increases rapidly above the MUF. Since this loss is closely associated with the MUF, the day-to-day variation of the MUF within the month can be used to estimate the day-to-day variation of these losses within the month. This loss due to partial failure of ionospheric support is referred to as an "over-the-MUF" loss[Equation (5.12)]. Since the basic loss equations contain the average effect of deviative absorption, an additional loss is only added to the high-angle modes (including those F modes on the upper side of the E MUF (see Equation 41). Sporadic-E mode losses are determined as are the regular E modes, but the deviative loss is zero and the over-the-MUF loss is what is usually termed reflection loss [Equation (5.13)].

The equations referred to provide monthly median losses when used with monthly median parameters of the ionosphere. In order to evaluate the performance of a communication system, the distribution of these losses within the month is needed. These distributions have been given as tables of transmission loss distributions (CCIR 252-2, 1970) and are uniform for operation frequency and for mode type. For geomagnetic latitudes below 40 degrees, these tables are for frequencies less than the FOT and are the variation of the F2 mode losses about the CCIR 252-2 equation based on 83 circuit years of data (Laitinen and Haydon, 1950). The rest of the tables correspond to 10.0 MHz and is based on the difference between minimum loss during the month and the distribution of losses above this difference within the Arctic regions. These tables are used in the following manner; the frequency that corresponds to the table of losses is established as either the F2 FOT or as 10.0 MHZ. Then the sporadic-E obscuration loss and the F2 over-the-MUF loss are subtracted from the table value. The residual table values are then added to the losses at each frequency for each mode. Auroral losses form the main part of the residual table. Decile values of losses are determined by calculating the Es obscuration loss and the over-the-MUF losses using the proper decile values of the Es and E, F1, or F2 mode MUFs. It should be especially noted in this model that the over-the-MUF losses limit the successful operation of the radio systems at the higher frequencies; i.e., the mode is always there but the losses become sufficiently high that the system becomes inoperative. The circuit reliability falls because of weak signal levels in contrast to earlier prediction methods which use a concept of "fraction-of-days" where the mode existed to limit the reliability at the higher frequencies. both the original table and the derived values are decibel with respect to the loss equations given here. If other loss equations are used, the distribution tables must be adjusted. the derivation of these loss equations is given below.

5.1 FREE-SPACE BASIC TRANSMISSION LOSS

Free-space losses result from the geometrical spreading of energy as the radio wave progresses away from the transmitter. In ionospheric propagation, the incremental cross section of the ray bundle at the receiver depends upon the physical properties of the ionosphere and the geometry of the propagation path. Simplifying asumptions are made in the program so that transmission losses can be calculated in a practical manner.

In the simplest model of sky-wave propagation, it is assumed that the earth and the ionosphere are both flat and that the reflection is specular (mirror-like). For this type of propagation, the energy density diminishes as the inverse square of the ray-path distance (Piggott, 1959). This means that for an isotropic transmitting antenna radiating p watts of power, the power flux density at a slant range distance D is $p/(4\ \pi\ D^2)$. The total area of an isotropic receiving antenna in free space is $\lambda^2\ /(4\ \pi)$, where λ is the wavelength of the radio wave. Therefore, the total power received by the antenna is $p\ \lambda^2\ /\ (4\ \pi\ D)^2$. The basic free-space transmission loss is the ratio between the power radiated and the power received by a loss-free receiving antenna, and is given by:

$$L_{bf} = 10 \log_{10} \left[\frac{p}{p\ l^2 / (4p\ D)^2} \right] = 20 \log_{10} \frac{4p\ D}{l} (dB)$$

(26)

Espressing the wavelength λ in terms of the frequency f of the electro-magnetic wave, (26) becomes:

$$L_{bf} = 32.45 + 20 \log_{10} f + 20 \log_{10} D \qquad (db)$$

(27)

where f is in Megahertz and D is in kilometers.

5.2 CCIR 252-2 IONOSPHERIC LOSS

The absorption in the D-E regions of the ionosphere is usually the major loss (after free space) in radio wave propagation via the ionosphere. To describe this effect, Martyn's theorem relating vertical and oblique path and the quasi-longitudinal approximation to the absorption loss (e.g., Budden, 1966) are used:

$$L(f_{ob}) = L(f_v)\cos f_0$$

(5.1)

$$L(f_v) = C\int_{h_0}^{h(f_v)} \frac{\frac{Nn}{m}\,dh}{(f_v + f_H)^2 + (\frac{n}{2p})^2}$$

(5.2)

where

C = constant,

h_o = height at bottom of ionosphere,

$h(f_v)$= height of reflection for frequency f_v,

N = N(h) electron density profile,

ν = ν(h) collision frequency,

μ = refractive index,

f_{ob} = oblique sounding frequency,

f_v = vertical sounding frequency,

f_H = gryofrequency, (f_L, the longitudinal component of gyrofrequency, is usually put into equation)

ϕ_o = angle of earth's normal to ray path at 100 km.

Equation (5.2) can be put into the form (Budden, 1966)

$$L(f_v) = (\nu/c)(h' - hp) \qquad (5.3)$$

where

ν = effective collision frequency

h' = virtual height of reflection,

hp = phase height of reflection,

c = velocity of light.

Since hp is bounded and h' is not, there is a strong dependence on frequency which cannot be explained simply by an inverse-frequency-squared law. The usual method of analysis has been to write equation (5.2) in the form (definition of the global absorption parameter A)

$$L(f_v) = \frac{A(f_v)}{(f_v + f_H)^2 + (n/2p)^2} \qquad (5.4)$$

Most analyses of absorption are based on estimated $A(f_v)$. This has sometimes been done by assuming non-deviative absorption only, and thereby trying to ignore the frequency dependence. When this is done with a small data base and no adjustment is made for the frequency dependence, the results can be misleading (and possibly inaccurate).

The CCIR absorption equation is based upon the U.S. Army signal Radio Propagation Agency study (Laitinen and Haydon, 1950), with a modification for lower frequencies by Lucas and Haydon (1966).

The exponent of the frequency term ($f_v + f_H$) and values for the terms $(\nu/2\pi)^2$ and $A(f_v)$ were determined by least square curve fitting. The oblique loss measurements were normalized to virtual loss measurements to give a standard comparison method, as well as to expand the data base, by the equation

$$L(f_{ob}) = \frac{L(F_v)[(f_v + f_L)^2 + (n/2p)^2]}{[(f_{ob} + f_H)^2 + (n/2p)^2]} \sec f_0 \qquad (5.5)$$

The data used were for F-layer modes only. The fitted equation is (see Figure 4).

$$L(f_{ob}) = \frac{677.2I \sec f_0}{(f_{ob} + f_L)^{1.98} + 10.2}$$

(5.6)

That is, the averaged value of $A(f_v)$ is

_ + 677.2I

where

I = -.04 + exp (-2.937 + 0.8445foE). (5.7)

The formula for absorption index I is in terms of foE which includes the variation in zenith angle and solar activity. This formula is an inversion of that formerly used to obtain foE from I. There have been attempts to modify and replace equation (5.6) by independent researchers. Schultz and Gallet(1970) (used in Barghausen et al., 1969) used the methods described by Piggott (1953) to describe _ without frequency dependence (non-deviative absorption) on a smaller data base than used to derive Equation (5.6), but did not add the frequency dependence suggested by Piggott (1953) [essentially the same as Equation (5.3), but for a parabolic E layer]. George (1971) has developed an absorption equation using an $A(f_v)$ which has an implicit $(h' - h_p)$ curve.

The method of supplementing equation (5.6) described below was based upon area coverage and radar backscatter data and was developed in two steps, first to correct equation (5.6) for E-layer modes and then for frequency dependence (deviative absorption). It is essentially based upon the suggestion in Piggott and in George, but with the advantage of having the electron density profiles available on a worldwide basis. (See also Rawer,1976; Bibl et al., 1961; and Fejer, 1961 for further discussion.)

5.3 FREQUENCY DEPENDENCE EFFECTS ON ABSORPTION

The absorption equation (5.6) contains an averaged value of $A(f_v)$ for F2-layer modes, i.e., the effects of E-region electron density on non-deviative absorption collision frequency (and magnetic field effects, etc.) were averaged in the curve fitting process. Therefore, a correction for E-layer modes was derived:

$$L_c = A + B \log_e (X_e), \tag{5.8}$$

where

L_c is the loss correction factor for E modes:

$A = 1.359$ for $f_oE > 2$ MHz,

$= 1.359\ (f_oE-0.5) / 1.5$ for $0.5 \leq f_oE \leq 2$ MHz,

$= 0.0$ for f_oE , 0.5 MHz;

$B = 8.617$ for $f_oE > 2$ MHz,

$= 8.617\ (f_oE - 0.5) / 1.5$ for $0.5 \leq f_oE \leq 2$ MHz,

$= 0.0$ for f_oE , 0.5 MHz;

$X_E = f_v / f_oE$ for $h > 90$ km,

$= f_v(90) / f_oE$ for $h \leq 90$ km;

h = true height of reflection;

f_v = equivalent vertical sounding frequency.

The equations for E-mode and F-mode losses assume that the mode goes through the absorbing region (true height of reflection above 95 to 100 km). Equation (38) represents the effect of E-layer losses which were included in Equation (36). When the true height of reflection is below 90 km, which will happen with the complete electron density profiles, the use of Equations (36) and (38) will give losses much higher than those observed. The absorption should reach a maximum as the operating frequency is lowered and then decreased. Theoretically the absorption reaches a maximum at the height where $\nu/2\pi = f + f_H$. However the electron density profile available does not represent the lower ionosphere adequately, so this behavior has been introduced into the model in an ad hoc manner by replacing the constant value of $(\nu/2\pi)^2 = 10.2$ by a calculated value.

When the true height of reflection, h,varies between 70 and 88 km the value of $(\nu/2\pi)^2$ varies between 40, the value it would have at a height of 61 km, and 10.2, the value it would have at a height of 64 km. The equation for the height h_ν is (h_ν does not correspond to any physical parameter)

$$h_\nu = 61 + 3(h-70)/18. \tag{5.9}$$

The equation for effective collision frequency is

$$(\nu(h_\nu)/2\pi)^2 = (\nu_o/2\pi)^2 \exp(-2(h_\nu-60)/H) \tag{5.10}$$

where

$$(\nu_o / 2\pi)^2 = 63.07$$

$$H = 4.39$$

The equation (5.10) gives realistic values for ν. The transformation from h to h_ν was derived using measured values of field strength on the Kogani to Akito path (Japan) at operating frequencies of 2.5 and 5.0 MHz, for the year 1970.

Since a complete electron density profile is used, any mode, high- or low-angle, will be considered. To account for the deviative (and spreading) losses of the high-angle modes, the following procedure is used. Deviative losses are considered to be averaged into Equation (5.6) for those modes with reflection heights less than that at the layer MUF. For modes with reflection height greater than that at the layer MUF and for modes just past the E-F cusp, a deviative loss term is added.

The equation is based on the relationship that the loss is proportional to the product of collision frequency with the difference between group path and phase path, i.e.,

$$A_p(f_v) = B(f_v)(h'-h)_N \sec(\phi_o), \quad (5.11)$$

where $A_p(f_v)$ is the deviative absorption loss in dB and

$B(f_v) = C_E \exp[-2(h-70)/ymE]$ for the E layer,
$= C_F \exp[-2(h-hmF2 + ymF2)/ymF2]$ for the F2 layer,
$B(f_v) = C_1 \exp[-2(h-hmF1 + ymF1)/ymF1]$ for the F1 layer and
$B(f_v) = C_2 \exp[-2(h-hmF2 + ymF2)/ymF2]$ for the F2 layer

when the F1 layer is present.

The constants have not been mapped on a worldwide basis as yet. Interim values used are

$C_E = 0.25$,
$C_F = 0.40$,
$C_1 = 0.60$,
$C_2 = B(foF1)$.

In order to preserve continuity at the F1-layer to F2-layer transition, C_2 is the value of $B(f_v)$ with f_v taken as foF1. This assures a smooth calculation of loss for all possible electron density profiles. Note that C_F and C_2 are forced to have minimum values of 0.05.

When sporadic E is present, the loss is supplemented by an Es obscuration factor as described in Section 5.4.

5.4 LOSS FOR PROPAGATION ABOVE THE STANDARD MUF

The model does not assume that propagation ceases at the junction frequency (or skip distance). It is known that the geometric optics approximation does not suffice in the neighborhood of the skip zone. By using wave methods, it is shown that energy difracts into the skip region (Bremmer, 1949). However, the observed signals are too strong to be explained in terms of wave propagation at the skip distance. The physical mechanism for the propagation of significant signals within the skip zone (or above the MUF when the distance is fixed) is not completely understood. One possibility is that the ray-path approximation for the calculation of skywave signal paths is probably inadequate since the skywave signal will normally return from a large region of the ionosphere (at least one Fresnel zone). As the frequency approaches the MUF, the energy arriving at the sharper angles will tend to penetrate and a portion of the Fresnel zone becomes ineffective as a reflector. As the frequency is further increased, less and less of energy is reflected and losses will sharply increase. On the longer paths where the fresnel zone is larger, losses increase slowly as the frequency exceeds the MUF compared to the sharp increase on shorter paths where the Fresnel zone is smaller. Other mechanisms may also contribute to the signal propagation and explain the significant signals observed above the MUF. For example, propagation may possibly be explained by scattering from horizontal irregularities in the ionosphere (Budden, 1966). The method used here is based on the empirical statistical method of Philips-Abel (Wheeler, 1966) rather than wave theory. The basic assumption is that a reflecting layer of the ionosphere may be considered as composed by quasi-random (quasi-independent) elemental patches of ionization. These elemental patches are considered to be composed of sub-patches, each with a classical MUF (JF). The median value of received power is proportional to the probability that there are reflecting areas with elemental classical MUF values that are equal to or greater than the transmission frequency. Experience indicates that the normal distribution is a fair estimate of the spatial probability of the elemental classical MUF values and that the mean value of this distribution is a fair estimate of the standard MUF. Further, at any given operating frequency there is some probability that the frequency will exceed the median monthly predicted MUF on some days. Thus this loss term includes both the effect of not being below the MUF on some days of the month and the loss on those days when the frequency is above the MUF. So this term is added at all operating frequencies.

The equation is

$$L = 10 \log_{10} P \sec(\phi) \quad \text{(dB)} \qquad (5.12)$$

where

$$P = \frac{1}{\sqrt{2p}} \int_Z^\infty \exp(-x^2/2)\, dx$$

$$Z = \frac{f_0 - fm}{s}$$

and

f_m is the MUF for the circuit elevation angle and distance (note that f_m is higher for a two-hop mode than for a one-hop mode on the same circuit). For vertical incidence, the loss is less than 0.5 dB for frequencies less than the FOT, and less than 3 dB for frequencies less than the MUF. Note that all modes from all layers (E, F_1, F_2, and E_s) now look the same (absorption losses plus over-the-MUF loss). The difference is in the distribution of the MUF's, being narrow for the E and F_1, somewhat wider for the F_2, and the widest for the E_s.

Since signal losses are associated with the ratio of the operating frequency to the MUF at a given time, the day-to-day distribution of expected losses near the monthly median MUF> As the frequency is well above the monthly median MUF; e.g., above the HPF only the scatter components remain and the signal is very weak, but the day-to-day distribution is not great.

5.5 Sporadic-E Losses

This section discusses the loss models associated with modes of propagation for which ray theory is not valid. The sporadic-E layer was not included in the electron density profile. It is modeled as a thin layer occurring at the height h'Es (usually 100 to 110 km). Its effect upon modes of propagation passing through it is given by Es obscuration loss. It is calculated by a method proposed by Phillips (1962) and modified to use the now available maps of foEs:

$$L_o = 10 \log_{10} (1 - P) \quad \text{(dB)} \tag{5.13}$$

where

$$P = \frac{1}{2p} \int_Z^\infty \exp(- X^2 /2)\, dx$$

$$Z = \frac{f_{ob} - f_m Es}{s} \ ,$$

$$f_m Es = foEs \sec f .$$

For modes which have reflected from the sporadic-E layer, the loss is the absorption losses supplemented by a reflection loss (corresponding to the over-the-MUF loss) defined by

$$L_R = 8.91\ p^{-0.7} \tag{5.14}$$

Note that this is effectively the same as $L_r = 8.91 - 10 \log(P)$ (dB).

5.6 SYSTEM LOSS

The system loss of a radio circuit is defined as the ratio of the signal power available at the receiving antenna terminals relative to that available at the transmitter antenna terminals, in decibels. This excludes any transmitting or receiving antenna transmission line losses, since such losses are considered readily measurable. The system loss does include all the losses in the transmitting and receiving antenna circuits - not only the transmission loss caused by radiation from the transmitting antenna and re-radiation from the receiving antenna, but also any ground losses, dielectric losses, antenna loading coil losses, and terminating resistor losses. Antenna gain is taken as antenna power gain which is the product of antenna directive gain in the direction aligned with the propagation path in both elevation and azimuth and of antenna efficiency.

The system loss is summarized as (Rice, et al., 1965)

$$L_b = L_{bf} + L_i + L_g - (G_t + G_r) \quad \text{(dB)} \tag{5.15}$$

where

L_{bf} = the basic free-space transmission loss expected between ideal, loss-free, isotropic, transmitting and receiving antennae in free space;

L_i = losses caused by ionospheric absorption, this term includes sporadic E obscuration loss, L_o , for F-layer modes. For all modes, this factor includes the deviative losses at high reflection heights, over-the-MUF loss as well as the tables of measured deviations which include auroral losses.

L_g = ground reflection losses.

G_t = transmitting antenna power gain relative to an isotropic antenna in free space;

G_r = receiving antenna power gain relative to an isotropic antenna in free space;

In this report, G_t and G_r are in the direction of the propagation path and include all antenna losses, so that $G_t + G_r$ is an approximation of the gain G_p . The values G_t and G_r are required for any elevation angle, azimuth direction, and frequency.

The skywave field strength is directly related to the transmission loss, L_b. This is the loss that would be observed if the actual antennas were replaced by ideal, loss-free, isotropic transmitting and receiving antennas. the field strength is:

$$E = 107.2 + 20 \log f_{ob} + G_t + P - L_b \quad (dB) \tag{5.16}$$

where

E = rem field strength in dB referred to one microvolt per meter,

G_t = transmitting antenna gain in the direction of the ray path used to determine L_s (decibels referred to an isotropic antenna),

P = transmitter power delivered to the transmitter antenna in decibels referred to one watt,

f_{ob} = operating frequency in megahertz.

In cases when the reference field strength is 300 millivolts per meter at one kilometer (rms field produced by 1 kw input to a short dipole over perfect earth), the skywave field strength, E, is

$$E = 142 + 20 \log f_{ob} - L_b \quad (dB) \tag{5.17}$$

Likewise, when the reference field strength is 222 millivolts per meter at one kilometer, the skywave field strength, E, is

$$E = 139.4 + 20 \log f_{ob} - L_b \quad (dB) \tag{5.18}$$

5.7 CONCLUSIONS

A semi-empirical method to include recent measurements, especially back-scatter measurement, in the calculation of ionospheric losses has been developed. It includes deviative and non-deviative effects as well as sporadic-E effects. The average effects of magnetic field and of polarization changes are included implicitly as the constants in the equations are taken from measurements which included these effects. The median excess system loss, Table 4 (Lucas and Haydon, 1966) is no longer used as it was mainly the average effect of sporadic-E and deviative losses.

6.0 LONG DISTANCE MODEL

A model to describe the virtual-height ray path and area coverage with single ionosphere reflections has been described (Section 5). This method was a combination of classical geometric-ray theoretical methods and empirical statistical methods. It has long been recognized that a continuation of such methods have severe limitations when applied to multi-hop propagation (Pedersen, 1927; Harnischmacher, 1960; Whale, 1969). As the radio path length increases, individual ray paths become increasing difficult to define, and the composite signal from all modes becomes increasingly important relative to the signal from an individual mode (Bremmer, 1949).

Even for short paths there may be significant contribution from multi-hop paths, especially when the antenna pattern does not favor the vertical angle associated with the single-hop mode. This is not necessarily an indication that there is anything basically wrong with the prediction techniques, but rather that there are fundamentally unpredictable (or random) factors present. The following section will describe some qualitative aspects of multi-hop propagation and a quantitative method for estimating the effect of the ionosphere upon multi-hops paths.

6.1 QUALITATIVE ASPECTS OF LONG DISTANCE PROPAGATION

The short-distance propagation model rigorously extended to long paths would lead to the expectation that failure of propagation at any of the ionospheric reflection areas would cause propagation to fail altogether. Empirically, however, it has been observed that propagation usually does not fail until ionospheric "control areas,' along the great circle path near each end of the path, fail to support transmission (CRPL, 1948). This is apparently true, within limits, no matter now long the great circle path is between the control points, and no matter what the condition of the ionosphere is in between.

Figure 10 illustrates some of the additional modes of propagation available over great distances along the great circle path. Actual propagation is not of course limited to a geometric plane, but travels by waves within some volume of space [hence we speak here of control 'areas" and reflection 'areas," not points, (see Figure 5)].

The modes depicted include chordal modes (i.e. those which because of ionospheric tilts are deflected over the absorbing regions) and M-modes, which reflect above a regular E- or sporadic-E layer on some part of the path. Any wave which leaves the earth and strikes the F2 layer excites scatter sources on its way up through the E region (short scatter), and on its way down, after being reflected from the F2 layer (long scatter). Re-radiation takes place from both regions. The short scatter source provides fairly intermittent energy because of the intermittent nature of the ionization causing the re-radiation. However, the wave reflected from the F2 layer is spread over a wide area so that there are enough patches of irregularities to provide an appreciable amount of re-radiation.

The irregularities consist of rather small departures of the electron density from the average of background value so the "blobs" in the ionosphere are not opaque, but are regions in which the refractive index is only slightly different from the average value. Such a medium can be referred to as a diaphanous screen (Whale, 1969). The power spectrum from such a medium contains two components: a pseudo-specular component and a scattered component. On short-distance paths, the specular component, which follows the geometric ray path, predominates. On long-distance paths, the scattered component becomes increasingly important. The situation is further complicated by horizontal and lateral inhomogeneities, presence of the magnetic field, and ground and ionospheric scatter, both along and from off the great circle path.

The proposed model for multi-hop propagation loss considers a wave which travels on a great circle path by considering three parts of this path:

- losses associated with the launching of a skywave from the transmitter,
- losses associated with the propagation of the wave between the launch and intercept area,
- losses associated with the intercept of a skywave at the receiver.

It is assumed that the effective launch area of the ionosphere may be identified by examining earth-ionosphere propagation paths and selecting the most efficient one as determined by combining the short-distance propagation model with appropriate transmitter antenna gains. The effective intercept area is determined in a similar manner using the appropriate receiving antenna gains.

It is assumed that between the launch and intercept areas the energy travels in a complex combination of specular reflection and scatter components (see figure 10), always seeking a path with the least loss.

In order to keep the models (single-hop and multi-hop) internally consistent, the single-hop models are used to estimate the launch and inherent areas of the multi-hop model and to estimate the losses between these areas. The following section gives a more detailed description

6.2 THE LONG-DISTANCE MODEL

Sampling areas are selected the same for both models; i.e., two at each end, and one in the middle. No new set of equations nor new computer code arises this way.

The basic transmission loss equation used in the single-hop model assumes continual divergence as if the medium were free space. A convergence factor is added to this equation for the multi-hop model. The theoretical angular (horizontal) convergence factor (Davis, 1965, 1969) is used and the resultant functional form is shown in figure 6.

C_H = 15 dB at the antipodal ($\Psi = \pi$)

$$C_H = 10 \log_{10}\left[\frac{P' \cos\Delta}{a \sin\Psi}\right] \qquad (6.1)$$

P' is the group path

where

C_H is the convergence factor, dB, and

Δ is the radiation angle,

a is the earth's radius,

Ψ is the distance angle.

Ionospheric losses for the multi-hop model are in three parts as follows:

(1) The loss associated with the launch of the skywave. The characteristics of the dominate launch path are taken from the samples of ionospheric parameters at the transmitter and of the circuit. The radiation angle of the transmitted ray is taken from that path which will have a maximum field strength at a ground distance of 4000 km. The ionospheric loss associated with the selected ray is then taken as one-half the loss associated with a one-hop mode using this ray. The distance corresponding to the launch of the skywave is one-half the ground distance associated with the one-hop mode.

(2) The loss associated with the intercept of the skywave. The dominant intercept path is assumed to be at the angle at which the ionospheric loss rate is the lowest; i.e., the least loss per kilometer of ground distance. As in the launch case, this angle and associated distance may be determined directly from the "ray set' table.

(3) Loss between the launch and intercept area. The distance between the launch and intercept areas is the great circle distance minus the distance to the launch area from the transmitter and the distance from the intercept area to the receiver. The loss rate along this distance is assumed to be approximated by the average of the loss rates at the three sample areas.

The model therefore assumes that absorption on long paths is related to the signal power that reaches the ionosphere at the transmitter end less the power that is attenuated at the receiver and less that power lost along the path. The expected behavior of the long-path model is depicted in Figure 7. For long-path propagation, the mode structure is lost, being a composite of ground and ionospheric reflection and scatter.

The total system loss for multi-hop propagation is then (figure 8)

$$L_T = L_{bf} - C_H + L_T + L_i + L_R + L_G + Y_P \qquad (6.2)$$

where

L_T is total system loss for long sky-wave paths.

L_{bf} is free space loss based on ray path distance.

C_H is a horizontal convergence gain.

L_T is loss in the launch of the radio wave at the transmitter. A combination of transmitter antenna gain and propagation losses for the most efficient mode at the sample area near the transmitter.

L_i is loss over the portion of the great circle path between the launch and intercept areas. Average of the loss rates at the sample areas times the distance between the launch and intercept areas.

L_R is loss in the intercept of the radio wave at the receiver. Calculated in the same way at L_T using receiver antenna gain.

L_G is an average ground loss rate times distance between launch and intercept areas.

Y_P is the prediction system loss correction factor which includes effect of auroral zones and sporadic E.

It is possible to designate the factor $A(f_v)$ in Equation (5.4) as a frequency term by defining a special lowest usable high frequency (LUF). Take the LUF as that value of frequency, f_{LUF}, where the field strength of 1000 kW of effective radiated power is 0 dBu (Beckmann, 1958). Combining Equations (30), (5.4), (5.15), (5.16), and (6.2), the field strength is

$$E = (E_0 + 34.8)\,[1 - L_T - L_i - L_R] + L_G + L_M + Y_P - 34.8 \qquad (6.3)$$

The reference field is E_o

$E_0 = 104.8 - 20 \log_{10} D$

L_M is the over-the-MUF losses from each end.

Rearranging the algebraic terms, the other factors are:

$$L_T = \frac{f_{L,T}^2}{f_0^{1.98} + 10.2} \qquad (6.4)$$

$$L_R = \frac{f_{L,R}^2}{f_0^{1.98} + 10.2}$$

$$f_{L,T}^2 = \frac{677.2\, I_T \sec f_T}{E_0 + 34.8}$$

(6.5)

$$f_{L,R}^2 = \frac{677.2\, I_R \sec f_R}{E_0 + 34.8}$$

(6.6)

I_T , I_R are absorption indices at each end of the path.

$f_o = f_{ob} + f_H$

$L_i = A_M\ D_M + A_F\ D_F$

D_M is the distance along the path supporting an M mode (Fig.14)

D_F is the total distance less D_M and the one-half hop distances at each end.

Using the night minimum absorption index (I = .1); an average distance factor (α) to replace the number of hops, and the loss per kilometer function, A_H is obtained from the rearrangement of the ionospheric loss Equation (5.6).

$$A_M = \frac{\left[\dfrac{19.335a}{(f_0^{1.98} + 10.2}\right]}{\left(D_M \log^{10}(b\,D)\right)}$$

$$A_F = \frac{\left[\frac{193.35a\ I}{f_0^{1.98} + 10.2}\right]}{\left(D_F \log_{10}(b\ D)\right)}$$

$$b = .1047\ 10^{7}$$

$$a = 1. + \frac{D_F - 4000}{D_F}, (\ use\ D_m)$$

(6.7)

I is average absorption index.

6.3 SUMMARY

The short-distance model based on a complete electron density profile of the D, E, F_1 , and F_2 regions with a separate sporadic-E layer predicts the ray path at any vertical angle of departure. Propagation losses for multipath propagation, which is essential for long paths, is considered to be approximated through a multiple application of the single-hop model. The steps are:

1. Sample the ionosphere at control areas near the transmitter and receiver and at the path midpoint.

2. Use the short-distance propagation model to develop a ray-set table at each sample location. This table includes propagation distance for each angle of departure including absorption and over-the-MUF losses.

3. Combine the transmitting antenna gain pattern with the propagation ray set for the sample area near the transmitter to determine the most efficient launch path for a distance of 4000 km. (Path with the lowest loss rate including transmitter antenna gain.) Note the launch loss (one-half the losses from the ray-set table plus

transmitter antenna gain) and the corresponding launch distance (one-half the ground wave range for a single hop).

4. Repeat #3 above to determine the most efficient intercept path using the sample area near the receiver and the receiving antenna vertical gain pattern.

5. Determine the distance between the ionospheric launch and intercept areas. (Ground great-circle distance minus the launch and intercept distance is an adequate approximation.)

6. Estimate a loss for the distance obtained in #5 above by averaging the loss rates at the three sample areas and multiply by the distance.

7. Determine the basic free-space loss and modify by a horizontal convergence factor.

8. Estimate ground losses (loss rate for type of intervening terrain times distance in #5 above).

9. Use the system loss adjustment factor table.

10. Combine 3, 4, 6, 7, 8, 9 to estimate the system loss.

7. HIGH-FREQUENCY SYSTEM PERFORMANCE

Two methods are used in the program to obtain estimates of the expected system performance. The first gives performance estimates in terms of the circuit reliability, which is defined as the fraction of days that successful communication may be expected at a given hour within the month at a specific operating frequency. The circuit reliability is based upon monthly median estimates of all operational parameters and their distributions and represents only the expected fraction of days in the month at the given hour that successful communication is expected. The second method gives estimates of the service probability, which is defined as the probability of obtaining a predetermined grade of service or better during a specified percentage of time (Barsis et al., 1961). It includes estimates of the prediction uncertainties associated with the operational parameters as a function of the percentage of time the specified grade of service is required, and it is therefore a measure of the chance of successful communication with the system employed.

7.1 CIRCUIT RELIABILITY

The primary factor in determining the circuit reliability is the signal-to-noise ratio, which is directly associated with a grade of service. The grade of service defines the quality of communication desired as, for example, the percentage of satisfied observers of facsimile transmissions. A minimum required signal-to-noise ratio is associated with the desired grade of service. This ratio is determined in terms of the class of emissions, modulation index, modulation rate, and signaling codes, and includes the effects of fading, error-correcting schemes, noise reducers, optimum modulation and detection techniques, and diversity schemes. The required signal-to-noise ratio for a minimum acceptable grade of service must be specified by the user.

The method for estimating the circuit reliability for a particular path consists of (1) calculating the maximum frequency that will be supported by the ionosphere; (2) determining the probability that a specified frequency will be propagated at a given hour within the month; (3) based on relationships between the specified system components and the propagation medium, calculating the distribution of signal-to-noise ratios from the medians and standard deviations of both signal power and noise power; (4) determining the probability that the signal-to-noise ratio will exceed the required signal-to-noise ratio; and (5) combining the two

probabilities to give an estimate of the circuit reliability.

The median value of received signal power P_e required for minimum acceptable grade of service during the month at a given hour is (CCIR, 1988)

$$P_e = F_{am} + R_{md} + B - 204 \text{ (dBW)} , \tag{7.1}$$

where

F_{am} = median of the hourly values of radio noise power density F_a within a seasonal time block system,

R_{md} = required system signal-to-noise power density ratio,

B = effective receiver bandwidth ($10 \log_{10} b$; b in Hz).

The values of F_{am} are given in terms of the effective antenna noise factor that results from the external noise power available from a loss-free antenna. Note that the values of F_{am} are representative of those that would be obtained with a short vertical lossless antenna over a perfectly conducting plane earth. Use of other antennas requires some correction because of directivity and polarization; it is not now accounted for in the program. To account for this, atmospheric noise source maps are now under study. The available signal-to-noise ratio $R_{S/N}$ at the receiving antenna terminals is calculated by combining the received signal power with the received noise power:

$$R_{S/N} = S - N, \tag{7.2}$$

where

S = monthly median signal in decibels,

N = monthly median of the hourly median radio noise power in decibels.

The probability $q_{S/N}$ that $R_{S/N}$ exceeds a given level is evaluated by the chi-square probability functions given by (5.20), where the value of χ^2 is related to R_{mo}. The median, upper, and lower decile values of the required signal-to-noise ratio, R_{mo}, $R_{.90}$, $R_{.10}$, respectively, are substituted in (5.21), (5.23), (5.24), and (5.26) for the MUF values, and the calculation proceed as before. The ratios $R_{.90}$ and $R_{.10}$ are defined as follows:

$$R_{.90} = R_{m_o} + 1.28 \, [\, s^{\,2}_{N_u} + S^2_u \,]^{1/2}, \tag{7.3}$$

$$R_{.10} = Rm_o - 1.28 \, [\, s_{\,N_\ell} + S^2_\ell \,]^{1/2}, \tag{7.4}$$

where

R_{m0} = median value D_{50} of the required signal-to-noise power ratio,

$\sigma_{Nu,l}$ = departures of the standard deviation of the radio noise from the median,

$S_{u,l}$ = departures of the standard deviation of the received signal from the median.

Values of N and 1.28 σ_N are obtained from numerical representations of the atmospheric, galactic, and man-made noise as described in section 4. Values of S(med.), S_u, and S_l are obtained by the methods described in section 7 in terms of the system loss and are shown in tables 7.3 and 7.4.

The probability q_f that at least one sky-wave mode will be present to produce the median available signal-to-noise is described in section 5, and the combined probabilities gives the circuit reliability

$$REL = q_f \, q_{S/N} \, . \qquad (7.5)$$

Therefore, the reliability is based on the available signal or signal-to-noise ratio and the fraction of days a sky-wave path is expected to be present. These two factors do not need to be associated with the same propagation mode, however. The program selects the lowest loss of all likely modes and combines this with the highest likelihood of ionospheric support to calculate the circuit reliability.

(a) the reliability computation is based (among other things) upon an estimate of the day-to-day variation in signal level;

(b) the semi-empirical determination of these day-to-day variations as used in this prediction method includes all modes of propagation (see sec. 7.4), i.e., signal levels associated with specific modes of propagation ate not separated out;

(c) the minimum loss (corresponding essentially to the highest hourly median signal level observed during the month) is more predictable than the monthly median of hourly medians, especially when predictions must be applicable worldwide;

(d) the minimum loss for any path is assumed to be associated with any mode that has a q_f of 0.01 or more; and

(e) the fraction of days for any propagation mode is assumed to be approximated by the fraction of days for the most probable mode.

The program lists the individual mode for any frequency and hour that has the highest reliability, but this particular mode may not be the mode with the lowest

loss or the highest likelihood of ionospheric support q_f used to calculate the circuit reliability. The lowest useful frequency (LUF) is defined as the minimum frequency at which the calculated circuit reliability is above a specified level. It has been common practice to designate the LUF as the minimum frequency with a circuit reliability of 0.90. An option is available in the program to specify any reliability level to designate the LUF.

7.2 SERVICE PROBABILITY

The service probability Q_t is the probability that the grade of service, g_r, defined by the required signal-to-noise ratio will be achieved or exceeded for a specified time availability, q_r. In other words, the problem is to assess the probability that the specified grade of service for a given percentage of the days within the month at some specified hour will be provided by the calculated available signal-to-noise ratio. Suppose, for example, that the fraction of days, q_r, within the month that the grade of service, g_r, is desired is 0.95, and that the calculated service probability is 0.70. This means that, for 0.95 of the days within the month, there is a 0.70 probability at the particular hour and frequency that the grade of service will be achieved.

Estimates of the service probability combine statistically the uncertainties of all values included in the prediction process. The most important of these are related to the prediction of the received signal and noise. The required signal-to-noise ratio, R_{mo}, that defines the grade of service, g_r, has an associated uncertainty because of errors in estimating equipment performance, short-term noise and signal variations, multipath propagation, etc. In the absence of sufficient test data, this uncertainty, expressed as a standard deviation, σ_r, has arbitrarily been taken to be equal to 2 dB for all grades of service.

Prediction uncertainties associated with estimates of the received signal level or, conversely, the excess system loss, are shown in table 4 and 5. Values represent estimates of the uncertainty, expressed as a standard deviation in predicting the median, σ_P, the upper decile σ_{Su}, and the lower decile σ_{Sl} of the excess system loss. These estimates of prediction uncertainties were obtained from comparisons of predicted values of received signals with those observed on operating circuits (R.M. Davis, 1969, private communication).

TABLE 4 EXPECTED EXCESS SYSTEM LOSS (dB)

(Paths Less than 2500 km)

WINTER (NOV., DEC., JAN., FEB.)

G.M.	01-04 LMT			04-07 LMT			07-10 LMT			10-13 LMT			13-16 LMT			16-19 LMT			19-22 LMT			22-01 LMT			G.M.
LAT.	Med	Sl	Su	Med	Sl	Su	Med	Sl	Su	Med	Sl	Su	Med	Sl	Su	Med	Sl	Su	Med	Sl	Su	Med	Sl	Su	LAT.
00-40	9.0	4.0	9.0	9.0	4.0	7.6	9.0	4.0	7.6	9.0	4.0	6.4	9.0	4.0	6.4	9.0	4.0	7.6	9.0	4.0	7.6	9.0	4.0	9.0	00-40
40-45	9.4	4.3	9.0	9.3	4.3	8.3	10.1	4.6	8.6	9.1	4.5	7.1	9.1	4.2	6.2	9.6	4.6	8.1	9.7	4.6	7.9	9.3	4.2	9.1	40-45
45-50	9.9	4.7	9.1	9.6	4.6	9.0	11.2	5.2	9.6	9.2	5.1	7.8	9.2	4.4	6.5	10.2	5.2	8.6	10.5	5.2	8.3	9.6	4.5	9.2	45-50
50-55	10.3	5.1	9.2	10.0	5.0	9.7	12.2	5.9	10.7	9.3	5.7	8.7	9.4	4.6	6.9	10.8	5.8	9.1	11.3	5.8	8.7	9.9	4.8	9.3	50-55
55-60	11.0	5.3	10.0	13.5	6.7	9.6	15.6	8.2	14.6	10.4	5.0	10.6	9.8	4.8	7.2	11.7	6.5	9.0	12.0	5.4	10.6	11.0	5.1	9.5	55-60
60-65	16.0	8.0	13.5	25.0	12.7	13.0	23.0	12.3	23.7	12.6	6.8	20.5	11.0	5.8	8.7	15.8	8.3	14.1	18.8	8.9	17.2	15.6	7.2	9.9	60-65
65-70	15.2	7.7	14.6	24.6	13.5	13.2	21.8	11.8	22.5	11.3	6.0	22.0	10.5	5.4	8.2	13.6	7.8	11.3	16.0	7.8	18.6	14.0	6.8	11.5	65-70
70-75	12.4	6.3	9.4	17.3	8.9	15.2	17.6	9.9	14.3	9.9	5.4	13.9	9.5	4.8	7.5	11.5	6.5	10.5	12.0	5.8	14.8	12.0	6.0	9.0	70-75
75-80	11.0	5.6	9.4	15.6	7.7	8.8	15.2	8.4	10.2	10.5	6.3	10.7	9.5	4.7	6.7	10.4	5.4	8.6	10.5	4.9	11.5	10.0	5.4	8.5	75-80

EQUINOX (MAR., APR., SEPT., OCT.)

G.M.	01-04 LMT			04-07 LMT			07-10 LMT			10-13 LMT			13-16 LMT			16-19 LMT			19-22 LMT			22-01 LMT			G.M.
LAT.	Med	Sl	Su	Med	Sl	Su	Med	Sl	Su	Med	Sl	Su	Med	Sl	Su	Med	Sl	Su	Med	Sl	Su	Med	Sl	Su	LAT.
00-40	9.0	4.0	9.0	9.0	4.0	9.0	9.0	4.0	7.6	9.0	4.0	6.4	9.0	4.0	6.4	9.0	4.0	7.6	9.0	4.0	7.6	9.0	4.0	9.0	00-40
40-45	9.5	4.5	10.0	9.6	4.4	11.5	10.6	5.3	9.8	10.0	4.7	9.0	9.7	4.5	8.9	10.3	5.0	11.3	10.0	4.8	10.0	10.3	4.7	10.0	40-45
45-50	10.1	5.0	11.1	10.3	4.8	14.1	12.3	6.6	12.0	11.0	5.4	11.6	10.4	5.0	11.4	11.6	6.0	15.0	11.0	5.6	12.5	11.6	5.4	11.0	45-50
50-55	10.7	5.6	12.2	11.0	5.2	16.6	14.0	8.0	14.3	12.0	6.2	14.2	11.2	5.6	13.9	13.0	7.0	18.7	12.0	6.4	15.0	13.0	6.2	12.0	50-55
55-60	11.4	5.7	17.6	13.4	6.4	22.0	16.5	8.3	15.3	14.0	7.6	18.3	11.6	5.6	15.5	13.8	7.5	20.2	14.5	7.7	19.5	15.1	7.4	13.3	55-60
60-65	15.7	7.7	30.3	20.2	9.5	29.3	26.0	14.0	23.4	18.0	10.6	33.0	16.2	8.3	19.2	18.0	10.3	27.0	19.9	11.3	29.0	24.0	13.0	26.7	60-65
65-70	15.5	8.1	28.0	21.0	11.1	31.0	30.4	18.2	26.9	17.5	10.0	27.9	13.8	7.0	18.0	15.0	8.4	24.0	19.0	11.3	28.8	22.7	11.3	17.5	65-70
70-75	12.3	7.0	21.7	20.0	13.8	20.8	20.6	12.8	20.2	14.1	8.8	18.9	11.6	6.2	14.2	13.0	7.2	18.0	15.0	8.6	22.0	16.0	8.0	16.5	70-75
75-80	10.4	6.1	15.5	11.5	7.5	18.7	16.4	9.7	14.4	12.8	7.5	13.6	10.0	5.4	12.0	11.4	6.2	14.1	11.4	6.4	20.6	12.3	6.3	15.7	75-80

SUMMER (MAY, JUNE, JULY, AUG.)

G.M.	01-04 LMT			04-07 LMT			07-10 LMT			10-13 LMT			13-16 LMT			16-19 LMT			19-22 LMT			22-01 LMT			G.M.
LAT.	Med	Sl	Su	Med	Sl	Su	Med	Sl	Su	Med	Sl	Su	Med	Sl	Su	Med	Sl	Su	Med	Sl	Su	Med	Sl	Su	LAT.
00-40	9.0	4.0	9.0	9.0	4.0	7.6	9.0	4.0	7.6	9.0	4.0	6.4	9.0	4.0	6.4	9.0	4.0	7.6	9.0	4.0	7.6	9.0	4.0	9.0	00-40
40-45	9.8	4.4	9.8	9.6	4.3	9.9	9.8	4.7	9.1	9.7	4.5	7.2	9.8	4.5	8.1	10.6	5.1	8.6	10.5	4.9	9.5	10.3	4.7	10.0	40-45
45-50	10.6	4.8	10.6	10.2	4.7	12.2	10.6	5.5	10.7	10.5	5.0	8.1	10.7	5.0	9.8	12.3	6.2	9.7	12.1	5.9	11.4	11.6	5.4	11.0	45-50
50-55	11.5	5.3	11.4	10.8	5.1	14.6	11.4	6.3	12.3	11.3	5.5	9.0	11.6	5.5	11.6	14.0	7.3	10.8	13.6	6.9	13.4	13.0	6.1	12.0	50-55
55-60	12.2	5.5	17.8	11.7	5.5	16.1	13.0	7.2	15.6	12.0	6.0	10.6	12.0	5.8	13.5	15.5	8.5	11.0	15.7	7.8	14.1	14.0	6.4	15.0	55-60
60-65	15.5	7.5	24.5	13.8	5.8	22.7	18.0	10.7	26.0	15.0	7.8	18.8	13.8	6.2	19.9	18.1	9.1	14.2	18.5	10.1	20.5	17.9	8.9	21.1	60-65
65-70	13.9	6.5	22.1	13.2	6.2	21.8	15.2	9.2	26.7	13.5	6.7	19.5	12.8	5.7	16.6	14.4	7.2	13.8	16.7	7.9	21.9	16.2	7.8	19.0	65-70
70-75	11.4	5.4	15.6	12.0	5.8	15.0	11.8	6.8	18.2	12.0	6.2	12.0	11.7	5.5	13.3	13.2	6.9	11.1	13.8	7.6	17.8	13.5	6.8	16.0	70-75
75-80	11.2	5.7	12.8	11.7	6.0	11.3	10.2	5.3	16.8	11.3	5.7	9.5	11.2	5.3	12.1	12.8	7.0	10.2	13.2	7.2	11.8	12.8	6.8	12.7	75-80

TABLE 4 EXPECTED EXCESS SYSTEM LOSS (dB) - Continued

(Paths Greater than 2500 km)

WINTER (NOV., DEC., JAN., FEB.)

G.M.	01-04 LMT			04-07 LMT			07-10 LMT			10-13 LMT			13-16 LMT			16-19 LMT			19-22 LMT			22-01 LMT			G.M.
LAT.	Med.	Sl	Su	Med.	Sl	Su	Med.	Sl	Su	Med.	Sl	Su	Med.	Sl	Su	Med.	Sl	Su	Med.	Sl	Su	Med.	Sl	Su	LAT.
00-40	9.0	4.0	9.0	9.0	4.0	7.6	9.0	4.0	7.6	9.0	4.0	6.4	9.0	4.0	6.4	9.0	4.0	7.6	9.0	4.0	7.6	9.0	4.0	9.0	00-40
40-45	9.3	4.2	9.1	9.3	4.3	7.8	9.4	4.2	9.0	9.0	4.2	7.3	9.0	4.0	6.5	9.3	4.3	7.7	9.5	4.3	7.6	9.4	4.3	9.2	40-45
45-50	9.6	4.4	9.3	9.6	4.6	8.0	9.8	4.5	10.4	9.1	4.4	8.2	9.1	4.1	6.7	9.6	4.7	7.8	10.0	4.6	7.6	9.5	4.6	9.4	45-50
50-55	9.9	4.6	9.5	10.0	5.0	8.2	10.3	4.8	11.9	9.1	4.6	9.2	9.1	4.1	6.9	10.0	5.1	7.9	10.5	4.9	7.6	10.4	4.9	9.6	50-55
55-60	10.6	4.7	9.6	11.4	5.5	8.3	11.7	5.6	12.4	9.6	5.2	10.4	9.4	4.6	7.4	10.7	5.5	7.6	10.8	5.0	7.9	12.5	5.3	9.8	55-60
60-65	14.3	5.7	11.4	16.0	6.8	9.5	14.9	7.3	14.1	11.0	5.2	15.2	9.7	4.1	8.3	13.0	6.7	8.0	13.5	5.6	8.9	19.0	7.8	13.8	60-65
65-70	14.5	6.5	10.2	14.0	6.3	10.9	16.0	8.3	14.2	10.9	4.4	15.8	9.5	5.1	7.7	12.0	6.2	7.3	13.5	6.1	8.5	18.6	8.6	11.1	65-70
70-80	11.5	3.4	9.7	13.5	6.5	7.8	13.3	6.8	11.2	9.8	4.8	11.2	9.3	4.7	7.1	10.6	5.4	7.4	11.0	5.1	8.6	13.8	6.5	9.2	70-75
80-85	10.5	5.1	9.2	11.7	5.9	8.1	11.5	5.7	10.2	9.8	4.8	9.2	8.8	4.4	7.0	9.9	5.0	7.5	9.8	4.8	8.2	10.6	5.0	9.7	75-80

EQUINOX (MAR., APR., SEPT., OCT.)

G.M.	01-04 LMT			04-07 LMT			07-10 LMT			10-13 LMT			13-16 LMT			16-19 LMT			19-22 LMT			22-01 LMT			G.M.
LAT.	Med.	Sl	Su	Med.	Sl	Su	Med.	Sl	Su	Med.	Sl	Su	Med.	Sl	Su	Med.	Sl	Su	Med.	Sl	Su	Med.	Sl	Su	LAT.
00-40	9.0	4.0	9.0	9.0	4.0	7.6	9.0	4.0	7.6	9.0	4.0	6.4	9.0	4.0	6.4	9.0	4.0	7.6	9.0	4.0	7.6	9.0	4.0	9.0	00-40
40-45	9.3	4.1	10.0	9.3	4.1	8.5	9.6	4.2	8.3	9.6	4.4	7.9	9.4	4.3	8.8	10.0	4.5	9.0	9.9	4.3	8.9	9.6	4.2	10.6	40-45
45-50	9.6	4.2	11.0	9.6	4.2	9.4	10.2	4.5	9.0	10.3	4.9	9.4	9.8	4.6	11.2	11.0	4.9	10.4	10.8	4.6	10.2	10.3	4.4	12.3	45-50
50-55	9.9	4.4	12.1	9.9	4.3	10.3	10.8	4.8	9.7	11.0	5.4	11.0	10.3	5.0	13.7	12.1	5.4	11.9	11.7	5.0	11.6	11.0	4.7	14.0	50-55
55-60	10.4	4.5	13.2	11.0	4.6	10.6	12.2	5.7	9.8	12.8	6.3	11.2	10.8	5.1	14.2	13.0	5.7	12.0	14.4	6.2	12.4	12.4	5.1	17.5	55-60
60-65	12.9	5.7	15.5	14.2	5.9	10.8	16.6	7.9	11.4	18.0	9.4	15.7	14.0	6.5	17.2	16.5	7.5	14.2	19.0	8.5	16.7	16.9	7.5	22.1	60-65
65-70	12.7	5.7	14.3	14.6	6.6	10.6	16.7	7.7	13.8	17.1	9.0	13.4	12.5	5.7	17.3	14.0	6.5	13.3	18.5	8.5	16.0	16.3	7.1	17.5	65-70
70-75	10.8	4.9	13.1	11.9	5.3	9.8	13.1	6.1	10.9	14.7	7.7	12.4	10.5	4.9	15.9	12.2	5.8	12.5	14.6	6.9	13.8	12.6	5.6	16.3	70-75
75-80	10.0	4.8	11.0	10.2	4.6	9.0	11.7	5.7	10.6	12.0	6.5	12.2	9.6	5.0	14.8	11.0	5.5	11.0	11.3	5.5	13.7	10.6	4.9	15.6	75-80

SUMMER (MAY, JUNE, JULY, AUG.)

G.M.	01-04 LMT			04-07 LMT			07-10 LMT			10-13 LMT			13-16 LMT			16-19 LMT			19-22 LMT			22-01 LMT			G.M.
LAT.	Med.	Sl	Su	Med.	Sl	Su	Med.	Sl	Su	Med.	Sl	Su	Med.	Sl	Su	Med.	Sl	Su	Med.	Sl	Su	Med.	Sl	Su	LAT.
00-40	9.0	4.0	9.0	9.0	4.0	7.6	9.0	4.0	7.6	9.0	4.0	6.4	9.0	4.0	6.4	9.0	4.0	7.6	9.0	4.0	7.6	9.0	4.0	9.0	00-40
40-45	9.7	4.4	9.1	9.8	4.4	9.1	9.7	4.5	8.1	9.3	4.2	6.9	9.7	4.5	7.6	9.4	4.2	8.1	10.4	4.9	8.2	9.8	4.4	9.6	40-45
45-50	10.4	4.8	9.2	10.6	4.9	10.6	10.4	5.0	8.6	9.6	4.4	7.5	10.4	5.0	8.8	9.8	4.5	8.6	11.9	5.8	8.9	10.6	4.9	10.3	45-50
50-55	11.2	5.2	9.4	11.4	5.4	12.2	11.2	5.6	9.2	10.0	4.7	8.1	11.2	5.6	10.1	10.2	4.8	9.1	13.4	6.7	9.6	11.5	5.4	11.0	50-55
55-60	11.8	5.4	9.6	12.8	6.2	13.0	12.7	6.5	9.7	10.4	4.9	9.2	11.7	5.9	12.3	10.6	5.1	9.7	13.5	6.8	11.8	12.2	5.7	13.4	55-60
60-65	14.5	6.7	9.8	17.5	8.8	16.8	16.6	9.3	13.8	11.6	5.6	13.1	13.2	6.8	17.4	12.2	6.1	11.3	14.5	7.1	17.2	14.7	7.2	18.4	60-65
65-70	13.4	6.1	10.0	15.3	7.4	16.7	14.9	8.2	14.5	10.9	5.4	13.1	12.3	6.3	14.0	10.7	5.4	10.4	13.4	6.4	15.2	13.5	6.4	15.1	65-70
70-75	10.9	4.8	8.9	13.6	6.5	11.9	11.9	5.9	11.1	10.3	5.0	10.1	11.2	5.5	12.2	10.3	5.1	9.0	11.8	5.8	12.3	11.7	5.3	12.1	70-75
75-80	10.9	5.3	8.2	12.8	6.0	10.0	11.2	5.5	10.1	10.1	4.8	8.6	11.1	5.4	11.4	10.2	5.0	8.2	11.3	5.6	9.9	11.4	5.5	10.3	75-80

TABLE 6. PREDICTION ERRORS IN THE ATMOSPHERIC RADIO NOISE LEVELS

Numerical Coefficients for use in Evaluation of the
Standard Deviation of the Median Value of the Atmospheric Radio Noise (σ_{FAM})

DEC - JAN - FEB

LMT	A1	A2	A3	A4	A5
00-04	.743379E+00	.184805E+01	-.890621E+00	-.199749E+01	.452507E+01
04-08	-.428242E+00	.302502E+00	.742824E+00	-.160900E+01	.417567E+01
08-12	-.342594E+00	.585453E+00	.177053E+01	-.985735E+00	.445041E+01
12-16	-.109963E+01	-.410156E+00	.272162E+01	-.191082E+00	.466347E+01
16-20	-.225828E+00	.262167E+00	.212719E+00	-.114419E+01	.468956E+01
20-24	.735803E+00	.143984E+01	-.177913E+01	-.191275E+01	.529731E+01

MAR - APR - MAY

00-04	.168882E+00	.653291E+00	.919879E-01	-.640683E+00	.367957E+01
04-08	.136798E+01	.256034E+01	-.222544E+01	-.292737E+01	.497452E+01
08-12	.114881E+01	.282530E+01	-.154909E+01	-.383357E+01	.603194E+01
12-16	.557917E+00	.171872E+01	-.111954E+01	-.284310E+01	.663045E+01
16-20	-.719275E-01	.119484E+01	.787773E+00	-.246763E+01	.451286E+01
20-24	-.104108E+00	.258124E+00	.256638E+00	-.575034E+00	.388959E+01

JUN - JUL - AUG

00-04	.441078E+00	.754692E+00	-.149459E+01	-.123047E+01	.552806E+01
04-08	.179997E+01	.285387E+01	-.427602E+01	-.421217E+01	.702824E+01
08-12	.122894E+01	.264191E+01	-.285556E+01	-.389196E+01	.766424E+01
12-16	.975428E+00	.875660E+00	-.440646E+01	-.204496E+01	.902340E+01
16-20	.147046E+01	.320094E+01	-.152498E+01	-.313552E+01	.587587E+01
20-24	.193233E-01	-.494468E+00	-.143067E+01	.118105E+00	.482582E+01

SEP - OCT - NOV

00-04	.507302E+00	.168124E+01	.292958E-01	-.211237E+01	.387806E+01
04-08	-.111661E-01	.110632E+01	.733434E+00	-.185950E+01	.449589E+01
08-12	.279820E+00	.177786E+01	.746844E+00	-.243937E+01	.494175E+01
12-16	.212440E+00	.130495E+01	-.603455E-02	-.221375E+01	.604906E+01
16-20	.820952E-01	.142235E+01	.685795E+00	-.248459E+01	.444219E+01
20-24	.425376E+00	.118228E+01	-.472298E+00	-.142879E+01	.427191E+01

TABLE 6. PREDICTION ERRORS IN THE ATMOSPHERIC RADIO NOISE LEVELS (CONT.)

Numerical Coefficients for use in Evaluation of the
Standard Deviation of the Upper Decile of the Atmospheric Radio Noise (σ_{DL})

DEC - JAN - FEB

LMT	A1	A2	A3	A4	A5
00-04	.126904E+00	.268785E-01	-.770942E+00	.226285E-01	.248548E+01
04-08	.614280E+00	.571794E+00	-.235541E+01	-.100525E+01	.404069E+01
08-12	-.119745E+00	-.151771E-01	-.408071E+00	-.438922E+00	.347453E+01
12-16	.248158E+00	.202147E+00	-.149445E+01	-.538425E+00	.379969E+01
16-20	.511612E+00	.347771E+00	-.232743E+01	-.632405E+00	.429346E+01
20-24	-.343668E+00	-.414469E+00	.343420E+00	.494973E+00	.241309E+01

MAR - APR - MAY

00-04	-.794447E-01	-.421282E-01	-.106715E+00	-.450397E+00	.275694E+01
04-08	.400025E+00	.417995E+00	-.156035E+01	-.869965E+00	.369667E+01
08-12	.996029E+00	.112322E+01	-.368354E+01	-.221057E+01	.577247E+01
12-16	.795788E+00	.912118E+00	-.388410E+01	-.251610E+01	.719725E+01
16-20	.416649E+00	.821670E+00	-.199945E+01	-.223434E+01	.521205E+01
20-24	.137420E+00	.572644E+00	-.345254E+00	-.150924E+01	.284754E+01

JUN - JUL - AUG

00-04	.232038E+00	.183979E+00	-.116380E+01	-.550627E+00	.294489E+01
04-08	.686566E+00	.435191E+00	-.290795E+01	-.878487E+00	.455870E+01
08-12	.760254E+00	.494537E+00	-.318959E+01	-.969695E+00	.499249E+01
12-16	.956414E+00	.375093E+00	-.436184E+01	-.729336E+00	.636323E+01
16-20	.680902E+00	.331788E+00	-.308260E+01	-.609270E+00	.496306E+01
20-24	.302133E-01	.200021E+00	-.166200E+00	-.521770E+00	.197852E+01

SEP - OCT - NOV

00-04	-.104326E+00	-.796536E-01	-.663268E-01	-.221128E+00	.244773E+01
04-08	.547742E+00	.505893E+00	-.187325E+01	-.747520E+00	.365203E+01
08-12	.927719E+00	.123641E+01	-.299950E+01	-.222166E+01	.514314E+01
12-16	.403634E+00	.695742E+00	-.198732E+01	-.177995E+01	.532871E+01
16-20	.148801E+00	.170572E+00	-.108537E+01	-.747057E+00	.383926E+01
20-24	.208183E-01	.125692E+00	-.290634E+00	-.662367E+00	.244939E+01

TABLE 6. PREDICTION ERRORS IN THE ATMOSPHERIC RADIO NOISE LEVELS (CONT.)

Numerical coefficients for use in Evaluation of the
Standard Deviation of the Lower Decile of the Atmospheric Radio Noise (σ_{DU})

DEC - JAN - FEB

LMT	A1	A2	A3	A4	A5
00-04	.586943E+00	.910163E+00	-.144586E+01	-.979273E+00	.320932E+01
04-08	.688151E+00	.149756E+01	-.147183E+01	-.217741E+01	.371525E+01
08-12	.667779E+00	.149891E+01	-.188272E+01	-.231266E+01	.518980E+01
12-16	.637561E+00	.154566E+01	-.159770E+01	-.217261E+01	.513591E+01
16-20	.272473E+00	.134363E+01	-.234189E+00	-.202113E+01	.372761E+01
20-24	.201483E+00	.709483E+00	-.493240E+00	-.963046E+00	.327557E+01

MAR - APR - MAY

00-04	.292770E+00	.588747E+00	-.399142E+00	-.827666E+00	.261711E+01
04-08	.121490E+01	.155130E+01	-.327356E+01	-.227474E+01	.483126E+01
08-12	.888091E+00	.104200E+01	-.334305E+01	-.175927E+01	.627552E+01
12-16	.510005E+00	.166035E+00	-.306647E+01	-.646328E+00	.690508E+01
16-20	.783329E+00	.768176E+00	-.290281E+01	-.155714E+01	.553903E+01
20-24	.239284E+00	.681585E+00	-.304964E+00	-.122301E+01	.269532E+01

JUN - JUL - AUG

00-04	.396174E+00	.566412E+00	-.116124E+01	-.792150E+00	.278700E+01
04-08	.787777E+00	.107465E+01	-.281629E+01	-.192217E+01	.480766E+01
08-12	.476864E+00	.300840E+00	-.257711E+01	-.614125E+00	.541123E+01
12-16	.294015E+00	-.609974E+00	-.290586E+01	.986589E+00	.631989E+01
16-20	.785736E+00	.705832E+00	-.332976E+01	-.124018E+01	.563061E+01
20-24	.576982E+00	.110841E+01	-.134597E+01	-.171088E+01	.270130E+01

SEP - OCT - NOV

00-04	.248494E+00	.485690E+00	-.744257E+00	-.847143E+00	.271592E+01
04-08	.846006E+00	.108394E+01	-.260229E+01	-.170798E+01	.439021E+01
08-12	.426888E+00	.161761E+00	-.255403E+01	-.525122E+00	.576006E+01
12-16	.350895E+00	.363107E-02	-.258306E+01	-.531405E+00	.598093E+01
16-20	.537617E+00	.877538E+00	-.189475E+01	-.172580E+01	.452224E+01
20-24	.160974E-01	.437416E+00	-.768397E-02	-.858681E+00	.262708E+01

Uncertainties in predicting the atmospheric radio noise are given in CCIR Report 322 (1988) as standard deviations representing the errors in predicting the median, σ_{Fam}, upper decile, σ_{Du}, and lower decile, σ_{Dl}. The curves representing the above variables were generated by a least squares fit with the polynomial (Lucas and Haydon, 1966)

$$Y(x) = A_1 + A_2x + A_3x^2 + A_4x^3 + A_5x^4, \qquad (7.1)$$

where

$Y(x)$ = σ_{Fam}, σ_{Dl}, or σ_{Du},

x = $\log_e f$,

f = frequency in megahertz.

The coefficients of the polynomial for each of the variables as a function of season, hemisphere, and time of day are given in table 6.

As already noted, the time availability, q_r, refers to the expected percentage of the hours in the month, used in defining the grade of service, during which the specified grade of service or better is achieved. The required grade of service is specified by a required signal-to-noise ratio and when this ratio is equaled or exceeded, the grade of service will be achieved. However, in calculating the available signal-to-noise ratio at the receiver, some allowance must be made for the variations of the hourly median signal levels and hourly median noise levels during the specified time period. This allowance is termed a protection factor (CCIR, 1988). The day-to-day variations in the hourly median signal level S and noise level N are assumed to be normally distributed and can be described by the median values and the deviation D_S or D_N from the median.

The protection factor, C, in decibels, necessary to provide the required signal-to-noise ratio, R_m, for the specified time availability, q_r, is determined, with no correlation assumed, from

$$C = \left[D_N^2 + D_S^2\right]^{1/2} \quad (dB) \qquad (7.2)$$

where

D_N = the value in decibels of the median noise power exceeded with a probability $(1 - q_r)$,

D_S = the value in decibels of the median loss exceeded with a probability (q_r).

Values of D_S and D_N are determined as follows. The standard normal variate ε, corresponding to a given value of q_r, is first obtained from a table in the computer program. Then,

$$D_N = \varepsilon D_u / 1.28 \quad (7.3)$$

$$D_S = \varepsilon S_u / 1.28 \quad (7.4)$$

for values of $q_r \geq .50$ and

$$D_N = \varepsilon D_l / 1.28 \quad (7.5)$$

$$D_S = \varepsilon S_l / 1.28 \quad (7.6)$$

for values of $q_r < .50$

The values of S_u (the difference between the excess losses exceeded 16 and 50 percent of the time) and the values of S_l (the difference between the excess losses exceeded 50 and 84 percent of the time) are given in tables 4 and 5. The upper decile D_u and the lower decile D_l of the median noise power (atmospheric, galactic, or man-made) are obtained by the methods described in section 5.

With the values of the required signal-to-noise ratio for the specified grade of service R_{mo}, and the required protection factor for the specified time availability C, the median value of the expected required signal power is (CCIR, 1988)

$$P_{me} = F_{am} \pm C + R_{m_o} + B - 204 \quad (dBW) \quad (7.7)$$

and is the equivalent of (8.1).

The prediction uncertainties are combined into a total uncertainty σ_t, on the assumption that the errors are un-correlated, from

$$s_t^2 = s_r^2 + s_P^2 + s_{F_{am}}^2 + s_C^2, \quad (dB), \quad (7.8)$$

where

σ_r = uncertainty in predicting the required signal-to-noise ratio R_m, standard deviation assumed to be 2 dB,

σ_p = standard deviation of estimates of the median received signal level

S,

σ_{Fam} = standard deviation of estimates of the median received noise level N,

σ_C = standard deviation of C and is composed of the standard error in predicting the radio noise level D_N and the signal level D_S corresponding to the given time availability; σ_C is a function of σ_{Su} (or σ_{Sl}) and σ_{Du} (or σ_{Dl}); therefore,

$$s_C^2 = \left(\frac{e^s D_{\ell,\mu}}{1.28} \right)^2 + (e\, s_{S_{\ell,\mu}})^2.$$

The service probability Q_t corresponding to the specified time availability q_r and a given required grade of service g_r is now calculated by the normal probability function.

The above service probability calculation is only valid for frequencies having a probability of ionospheric support q_f equal to one. for frequencies having a probability of support less than one, the total service probability would be

$$SPROB = Q_t \cdot q_f. \qquad (7.9)$$

Figure 8 illustrates the calculations described above that the program evaluates to obtain estimates of circuit performance based on the service probability concept. Remember that we are concerned with the system signal levels where the decile values $R_{.10}$ and $R_{.90}$ are the reverse of those associated with system losses. The two curves illustrate the distributions and service probability estimates for two different time availabilities q_r. The calculated available signal-to-noise ratio for the frequency and path is 57.5 dB. The probability of ionospheric support q_f for the frequency and path is assumed to be equal to one. Note that the higher time availability gives a lower service probability. When service probability is used as a prediction of the expected systems performance, the lowest useful frequency (LUF) may be defined as the minimum frequency at which the service probability is above a specified level.

7.3 Multipath Evaluation

The computer program contains a provision for calculating the likelihood of multipath on a given transmission circuit (Lucas and Haydon, 1966). It is an

important consideration for high-speed data transmission systems where interference due to multipath propagation can cause intolerable bit error rates (Bailey, 1959).

Multipath occurs when signals of comparable amplitude are propagated with different delay times via two or more paths with a different number of hops. It can occur a large percent of the time over a wide frequency range. The number of modes depends on the relationship of the actual operating frequency to the path MUF. At frequencies near the MUF, multipath is very low or entirely absent. As the operating frequency is decreased relative to the MUF, the likelihood of other modes being received is increased, and it is therefore desirable to have some indication of the presence of multipath for selecting operating frequencies.

If the operator has an adequate choice of frequencies to permit operation where the likelihood of multipath is low, an adequate signal-to-noise ratio will suffice to determine circuit performance. If the reliability or service probability of two frequencies is equal, and one has a greater likelihood of multipath, then the frequency with the lowest multipath is preferable. It is also possible to reduce multipath by antenna design or selection.

The probability of multipath is a function of frequency, path length, location, local time, and season. The program predicts the probability of multipath based upon some discrete minimum difference in received power and maximum tolerable delay time between modes. The probability of multipath is assumed to be the probability that a second sky-wave mode will be present to produce a minimum difference in received signal powers.

The minimum tolerable difference in received power and maximum tolerable delay time difference between modes are input parameters to the program and depend on the communication system used.

8. MAXIMUM USABLE FREQUENCY (MUF) MODEL

The maximum frequency which will support communications between two points is an important parameter in radio system design and operation. Because of the stochastic nature of the ionosphere, it is a very difficult parameter to determine. This communication analysis program follows the classical philosophy of determining a MUF based on monthly median ionospheric condition; i.e., to determine the frequency where the high and low angle rays merge JF (Junction Frequency) using a predicted ionosphere and to designate this frequency as MUF. Using the day-to-day distribution of F_2MUF (3000) (i.e., MUF at a distance of 3000 kilometers for the F_2 layer), the percentage of days a given frequency will be below the JF of the F_2 region can be estimated. Frequencies which will be below the JF 90 percent of the days are classically called optimum traffic frequencies (FOT) and those below the JF only 10 percent of the days are called highest probable frequencies (HPF). For the E and F_1 layers, the distribution is taken as normal with a standard deviation of 10 percent of the MUF.

The sampling of the ionosphere to determine the MUF is the same as it is for the rest of the models. For short paths, only the middle of the great-circle path is sampled. for long paths, the MUF is determined from the sample area with the lower ionization at the ends of the path. It should be noted that in this model communication does not fail at the MUF, only the signal level starts to sharply decrease as frequency is increased above the daily MUF.

The MUF calculated this way does not correspond to the maximum observed frequency (MOF) between two radio systems. The MOF may differ for any of several reasons: the ionosphere (e.g., foF2) may differ sufficiently from the median, the signal may be caused by an over-the-MUF mode or some other process such as ground scatter, or the signal may result from the sporadic-E mode. The 50 percent sporadic-E MUF is available as an optional output. The predicted MUF corresponds to a junction frequency, and is not normally measured. Note that no account of ionospheric storms nor of operational characteristics is taken in the calculation of the MUF. finally, note that the MUF is not the maximum frequency at which the program will predict a mode existing between two points on the earth's surfaces. High-angle rays, over-the-MUF modes, and possible E_s modes will predict existing frequencies over the predicted MUF.

8.1 GEOMETRY OF THE MUF (JF)

A straightforward method to find the MUF would be simply to evaluate the complete electron density profile, integrate to find the corresponding virtual heights, and then use some search technique to find the predicted junction frequency. In order to simplify the calculations, an alternate procedure has been devised which is basically an extension of Lucas and Haydon (1966). The major insight is to devise a method of finding the junction frequency curve as a function of the ionospheric distance, and frequency. The basic parameter is X_T, the ratio of the tangent frequency f_t to the critical frequency of the layer (e.g., foF1). The term tangent frequency comes from the manual method of transforming a vertical incidence ionogram into an oblique ionogram for a given distance using a transmission curve. The JF curve is approximated in three steps. First the equivalent vertical sounding frequency corresponding to the JF, F_t, is estimated using the equation:

$$ymE = \frac{hmE}{5.5} = \frac{110}{5.5} = 20.0 \qquad (8.1)$$

where

X_t is the ratio of f_t to the layer critical frequency,

f_t is to correspond with the tangent point on the ionogram when using the transmission curves (NBS, 1948),

y_m is the semi-thickness of the layer,

h_m is the height of maximum ionization of the layer,

α is an adjustment factor (α = 0.5).

For α = 1, Equation (8.1) is the equation for the point on the ionogram corresponding to minimum time delay for propagation over a spherical earth and in a flat ionosphere. When the corrected Martyn's theorem (see Section 3.7.4) is used, X_t

starts at the flat ionosphere value for zero distance and approaches the JF value for longer distances. A value of α = 0.5 approximates the JF line somewhat better with the ionosphere used in the program. For the F_2 layer, a correction to X_t is used to force the MUF to approach the zero MUF as a function of distance:

$$X_t = X_t (1 + A \exp(-B\, D/ D_o)) \tag{8.2}$$

where

X_t is modified (i.e., as in FORTRAN),

$A = -1. + 1./X_t$,

$B = 9.5$,

D = ground distance,

D_o = base distance (2000 km).

The JF curve given by Equation (8.2) with force the curve to rise (or fall) much more sharply than the actual curve, thus giving a more conservative estimate of the MUF. Note that the modified X_t approaches 1. at zero distance and approaches the original value of X_t at D_o .

The distinction between long paths and short paths exists for the MUF calculation also. For long paths, the MUF is that corresponding to an elevation angle of zero or the minimum angle desired. An electron density profile is generated, X_t is calculated for each layer, table lookup is used to find the true height, and the secant law is used to find the MUF (no correction factor as the true height is used). The relevant equations are:

$$f_t = X_t\, f_c \,, \tag{8.3}$$

where

f_t = vertical tangent frequency,

X_t = is given by Equation (57),

f_c = zero MUF,

= foE for E layer,

= foF1 for F1 layer,

= foF2 + 1/2 f_H for the F2 layer,

f_H = gyrofrequency.

For the short path, the mode structure must be determined. This implies calculation of the elevation angle, and thus use of the corrected form of Martyn's theorem. The latter implies an integration of the electron density profile and an iteration for the virtual height. For the E layer, the correction to Martyn's theorem is small and may be omitted. The equations are:

$$N = [\, D/(\,(\,p/2 - \Delta - f'\,)a)] + 1 \qquad (8.4)$$

where

N = number of hops. ([ ] here implies truncation and the first Δ is zero or minimum takeoff angle Δ),

D = ground distance,

a = earth radius,

ϕ' = angle at virtual height h',

ψ = hop distance angle,

ϕ = angle at true height h^T,

f_t = vertical tangent frequency.

For the E layer, using the parameters ymE = 20, hmE = 110 (which can be changed by user via input), the value of X_t is

X_t = .957,

which gives, using the electron density profile described in Section 3,

h_T = 104 as true height, and

h' = 130 as virtual height.

For the F1 and F2 layers, Equation (8.3) and (8.4) are used to find an initial (h' , Δ) pair. Then the virtual height is corrected (as for corrected Martyn's theorem) and a new Δ and MUF is found. This corrective procedure is repeated until the change is MUF is less than a specified value or until a maximum number of iterations have been performed (only one repetition normally results).

The sporadic-E MUF is found using the predicted foEs and the secant factor with the true height and virtual height taken as equal (normally 110 km in the program).

9. ACKNOWLEDGEMENTS

This report is the result of the efforts of many groups and individuals. It is a technical description of ICEPAC with orientation toward the PC computer use. The wording is sometimes an extraction of reports describing the scientific basis for this program. In regard to individuals, the following list may not include everyone, but hopefully the majority will be mentioned. The author wishes to acknowledge the contributions of Mr. J. Washburn, Mr. A.F. Barghausen, Dr. Mark T. Ma, Mr. D.H. Zacharisen, Dr. E.L. Crow, Mr. G.W. Haydon, Mr. D.L. Lucas, Mr. J.L. Lloyd, Mr. G.R. Hand, Dr. A.D. Spaulding, Dr. R.K. Rosich, Mr. L.R. Teeters, Mr. R.M. Davis Jr., and many others who have been instrumental in the evolution of the propagation programs and documentation.